© 2019. Published by The Company of Biologists Ltd | Development (2019) 146, dev175810. doi:10.1242/dev.175810

RESEARCH ARTICLE

Yap and its subcellular localization have distinct compartment-specific roles in the developing lung

Benjamin J. van Soldt[1], Jun Qian[1], Jiao Li[2], Nan Tang[2], Jining Lu[1] and Wellington V. Cardoso[1,*]

ABSTRACT

Although the Hippo–yes-associated protein (Yap) pathway has been implicated in lung development, the specific roles for Yap and its nucleocytoplasmic shuttling in the developing airway and alveolar compartments remain elusive. Moreover, conflicting results from expression studies and differences in the lung phenotypes of Yap and Hippo kinase null mutants caused controversy over the dynamics and significance of Yap subcellular localization in the developing lung. Here, we show that the aberrant morphogenesis of Yap-deficient lungs results from the disruption of developmental events specifically in distal epithelial progenitors. We also show that activation of nuclear Yap is enough to fulfill the Yap requirements to rescue abnormalities in these lungs. Remarkably, we found that Yap nucleocytoplasmic shuttling is largely dispensable in epithelial progenitors for both branching morphogenesis and sacculation. However, if maintained transcriptionally active in airways, nuclear Yap profoundly alters proximal-distal identity and halts epithelial differentiation. Taken together, these observations provide novel insights into the crucial importance of Hippo-Yap signaling in the lung prenatally.

KEY WORDS: Yap, Branching morphogenesis, Airway differentiation, Progenitor cells, Lung development, Alveolar differentiation

INTRODUCTION

The generation of organs with complex three-dimensional (3D) tubular architecture and distinct functional compartments, such as the mammary gland, kidney and lung, requires coordinated activation and integration of multiple signaling networks. Yes-associated protein (Yap), a key effector of the Hippo pathway, has been increasingly recognized as a crucial player in this network for its ability to integrate mechanical and chemical signals to control cell behavior during organogenesis (Mauviel et al., 2012; Varelas, 2014; Yu and Guan, 2013). Yap activity is largely dependent on its phosphorylation status, an event controlled by Hippo kinases, including mammalian STE20-like protein kinase (Mst; also known as Stk3) and large tumor suppressor (Lats). Yap phosphorylation on serines (S127 in humans and S112 in mouse) alters its subcellular localization, favoring cytoplasmic retention and, thus, restricting Yap transcriptional output. The nucleocytoplasmic shuttling of Yap is a highly dynamic process, particularly in Yap-expressing structures undergoing rapid morphogenetic changes. However, differential activity of Hippo kinases leads to preferential subcellular localization of Yap in distinct groups of cells or compartments (Manning et al., 2018). This acts as a crucial mechanism to ensure that a proper balance of the Yap transcriptional and cytoplasmic activities is achieved in a particular compartment, preventing Yap-mediated aberrant cell behavior, as observed in cancer (Zhang et al., 2015; Zhao et al., 2011).

Yap and Hippo kinases are expressed in the embryonic lung from early developmental stages in both epithelium and mesenchyme (Lange et al., 2015; Lin et al., 2015; Mahoney et al., 2014). Previous studies demonstrated that Hippo-Yap signaling has an important role in the adult lung, mediating regeneration-repair responses in several injury models (Liu et al., 2016; Otsubo et al., 2017; Volckaert et al., 2017; Zhao et al., 2014). Notably, there is also evidence that this pathway is crucial for lung organogenesis. This was first recognized by studies of severely hypoplastic lungs with truncated airways and distal cysts reported in sonic hedgehog (Shh)^{Cre};$Yap^{flox/flox}$ ($Yap^{f/f}$) mutants in which Yap was inactivated in the foregut endoderm at the onset of lung development (Mahoney et al., 2014). Shh^{Cre}-mediated deletion of Mst1/2 or Lats1/2, leading to the expected nuclear Yap accumulation from the loss of Hippo kinase function, also resulted in disruption of lung development. However, the lung phenotypes differ markedly between these mutants (Lange et al., 2015; Lin et al., 2015; Nantie et al., 2018). Lats1/2-null lungs were severely hypoplastic and had major defects in branching morphogenesis, reminiscent of that seen in Yap-deficient lungs. By contrast, no branching defects were apparent in Mst1/2 mutants, which rather showed abnormal distal differentiation despite displaying the same accumulation of nuclear Yap seen in Lats1/2 mutants.

These observations raised questions about the extent to which these kinases overlap in function and whether the lung abnormalities of these mutants resulted solely from the inability of Yap to shuttle to the cytoplasm or included unrecognized non-Yap-related effects of Mst/Lats deficiency. More fundamentally, information was missing about the role of Yap and its nucleocytoplasmic shuttling in compartment-specific events in the absence of potential confounding effects of Hippo kinase inactivation. Lastly, evidence of the preferential localization of Yap in the nucleus or cytoplasm of the developing lung has been inconclusive because of conflicting results from different reports (Lange et al., 2015; Lin et al., 2015, 2017; Mahoney et al., 2014; Nantie et al., 2018; Szymaniak et al., 2015). Although informative, these studies revealed major gaps of knowledge and left key questions open. Are there specific roles for Yap as the airway and distal lung compartments form and differentiate? If so, do these compartment-specific functions depend on a particular subcellular distribution of Yap in the nucleus or cytoplasm? How would lung development be affected by the inability of Yap to undergo nucleocytoplasmic shuttling in epithelial progenitors?

Here, we provide functional evidence of distinct compartment-specific requirements for Yap in the developing lung. We show that

[1]Columbia Center for Human Development, Department of Medicine, Pulmonary Allergy Critical Care, and Department of Genetics and Development, Columbia University Medical Center, New York, NY, 10032, USA. [2]National Institute of Biological Sciences, Beijing 102206, China.

*Author for correspondence (wvc2104@cumc.columbia.edu)

W.V.C., 0000-0002-8868-9716

Received 14 January 2019; Accepted 28 March 2019

Development (2019) 146, dev175810. doi:10.1242/dev.175810

activation of a Yap nuclear transcriptional program is enough to fulfill all Yap requirements essential to form the distal lung. Remarkably, we found that nucleocytoplasmic shuttling is largely dispensable for both branching morphogenesis and sacculation but is crucial for airway differentiation. These observations provide novel insights into the role and regulation of Yap in the developing lung.

RESULTS

Yap is required in the Sox9+ but not in the Sox2+ compartment for lung morphogenesis

To dissect the compartment-specific role of Yap during lung development, we disrupted Yap expression specifically in either distal or (proximal) airway progenitors, once the sex determining region Y-box 9 (Sox9) and the Sox2 domains were clearly established in these compartments. *Sox9*^{CreERT2};*Yap*$^{f/f}$ mice were generated and tamoxifen (TMX; 5 mg) was administered sequentially to pregnant mothers at embryonic day (E)11.5 and E12.5. Embryos were analyzed every other day up to E18.5. Morphological analysis revealed no obvious gross abnormalities or differences in body size in mutant mice compared with their no-*Yap*$^{f/f}$ control littermates (data not shown). However, lungs from homozygous mutants showed progressively severe cystic expansion of the distal compartment with increasing developmental stage (Fig. 1A). These changes were already noticeable by E14.5 and, by E18.5, the overall morphology of *Sox9*^{CreERT2};*Yap*$^{f/f}$ lungs was highly reminiscent of that resulting from global deletion of Yap in *Shh*^{Cre};*Yap*$^{f/f}$ mice (Mahoney et al., 2014) as

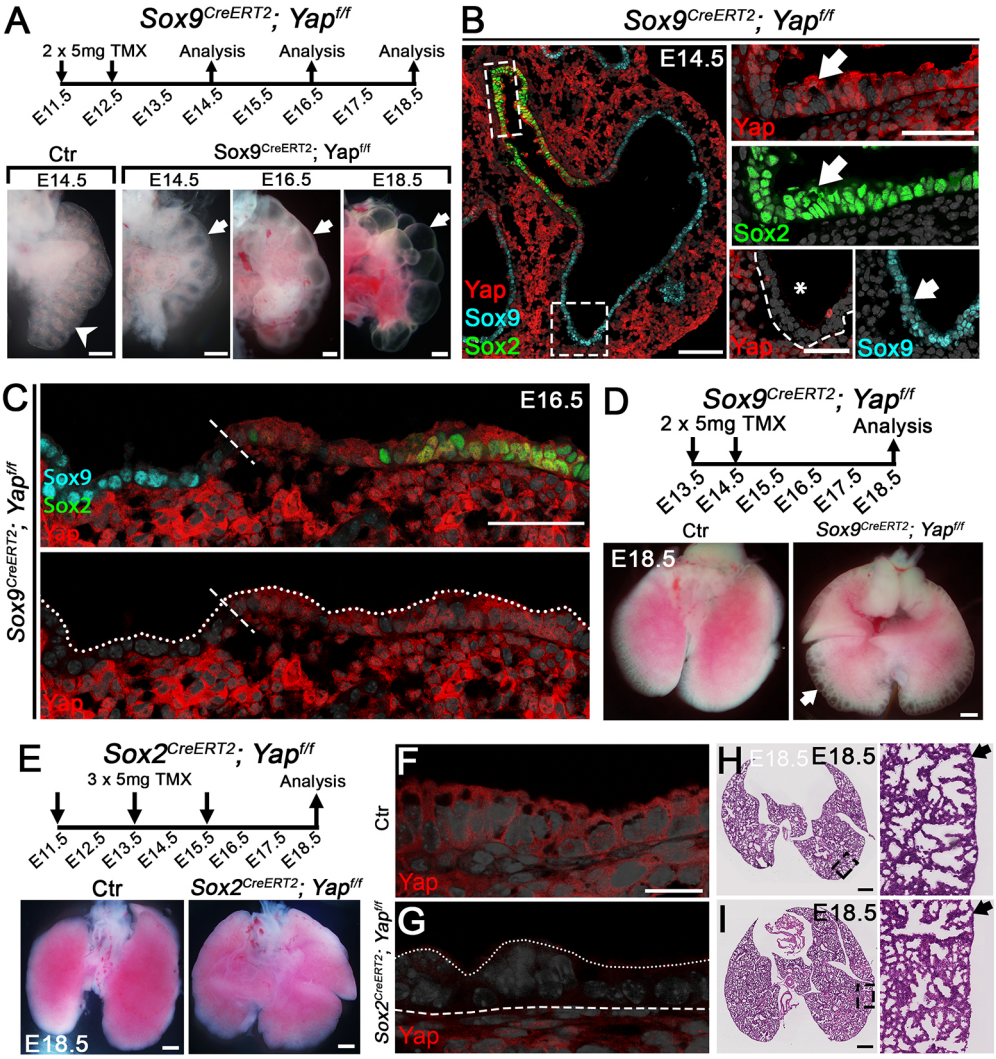

Fig. 1. Yap is required in the Sox9+ progenitor compartment, but not in the Sox2+ airway compartment, to form distal branches and initiate airway morphogenesis. (A) Schematic of the experimental design: TMX administration and analysis of *Sox9*^{CreERT2};*Yap*$^{f/f}$ mutants (top); whole-mount images of left lungs (bottom): normal distal branches in control (Ctr) lungs (E14.5, arrowhead) and aberrant distal cyst in mutant mice (E14.5-E18.5, arrows). (B,C) IF of Sox2, Sox9 and Yap in *Sox9*^{CreERT2};*Yap*$^{f/f}$ lungs showing compartment-specific disruption of Yap in distal (Sox9+) but not in proximal (Sox2+) epithelium (note preserved Yap throughout the mesenchyme). (B) E14.5 mutant lungs: high-resolution panels in B (right) depict boxed areas enlarged from overview (left); asterisk denotes the lack of Yap in the distal compartment. Arrows indicate a Yap+ cell that is also Sox2+ (top and middle), and Sox9 positivity in the Yap− cell (bottom). (C) E16.5 mutant lungs: transition between the distal and proximal compartments (dashed line) showing consistent Sox2 expression only in areas not targeted by *Sox9*^{CreERT2}. Dotted line denotes the luminal aspect of the epithelium. (D) Late TMX administration to *Sox9*^{CreERT2};*Yap*$^{f/f}$ mutants (schematic indicates the experimental design). Whole-mount images of E18.5 Ctr and mutants showing small distal cysts in mutants (arrow). (E-I) TMX administration and analysis of *Sox2*^{CreERT2};*Yap*$^{f/f}$ mutants. Whole-mount (schematic indicates the experimental design) (E) and Yap IF (F,G) analyses of E18.5 Ctr and mutant lungs: normal gross morphology and efficient Yap deletion in the airway epithelium of mutants. (H,I) H&E staining of E18.5 Ctr and *Sox2*^{CreERT2};*Yap*$^{f/f}$ lungs showing histologically comparable distal saccules (arrows in boxed areas enlarged). Dashed and dotted lines in G outline the basement membrane and apical aspect of the epithelium, respectively. DAPI appears gray in all panels. Scale bars: 500 µm in A,D,E; 100 µm in B (overview), F,G; 50 µm in B (insets), C; and 20 µm in H,I.

Development (2019) 146, dev175810. doi:10.1242/dev.175810

well as from distal Yap deletion using a constitutive Cre (*Sox9^{Cre};Yap$^{f/f}$*) reported previously (Lin et al., 2017).

Immunofluorescence (IF) analysis confirmed the selective epithelial inactivation of Yap in the distal cyst-like structures. Although negative for Yap, the epithelium remained strongly labeled for Sox9 (Fig. 1B), further supporting the distal origin of the cysts. Moreover, Yap deletion in the Sox9+ progenitor cell population had no apparent effect on the expression of key early distal cell markers [Sox9, surfactant-associated protein C (Pro-SPC; also know as Sftpc) and bone morphogenetic protein 4 (Bmp4), Fig. S1A], supporting previous observations in *Shh^{Cre};Yap$^{f/f}$* mice (Mahoney et al., 2014). By contrast, Sox2 was invariably absent from the Yap-deficient epithelium and was seen only more proximally in Yap-expressing areas unaffected by *Sox9^{CreERT2}*-mediated recombination (Fig. 1B,C). Interestingly, Sox2 was clearly detected in the intrapulmonary airways of *Sox9^{CreERT2};Yap$^{f/f}$* mutants. However, signals were restricted to the areas of preserved Yap expression, suggesting that the Sox2+Yap+ airway progenitors had been already specified before TMX treatment (E11.5) and, thus, were unlikely to have been generated from Yap-deficient Sox9+ progenitors (Fig. 1B,C). Indeed, TMX administration later in development (E13.5 and E14.5) still resulted in disruption of distal morphogenesis, although the phenotype was much milder: E18.5 lungs only had small distal cysts and mild hypoplasia (Fig. 1D).

We next examined the role of Yap in epithelial buds once Sox2 expression had been established. A previous study proposed Yap to be uniformly active throughout the developing lung epithelium (Lin et al., 2017). Consequently, faulty morphogenesis (as cysts) because of Yap deletion was predicted to occur anywhere along the proximal-distal axis of the developing lung epithelium. We reasoned that, if true, this should be confirmed using a *Sox2^{CreERT2};Yap$^{f/f}$* mouse model. Thus, TMX (5 mg) was administered to these mutants at gestational days 11.5, 13.5 and 15.5, and embryos were examined at E18.5 (Fig. 1E). Gross morphology showed that E18.5 Yap-deficient lungs were indistinguishable from those of their *Yap$^{f/f}$* control littermates (Fig. 1E). Efficient targeting was confirmed by the absence of Yap throughout the Sox2+ airway epithelium (Fig. 1F,G). Histological analysis and IF for Sox2/Sox9 showed no obvious defect in branching morphogenesis or proximal-distal patterning in developing airways (Fig. 1H,I; Fig. S1B,C). The distal compartment was histologically comparable with normal saccules populated by both alveolar type 1 and type 2 (AT1, AT2) cells, in sharp contrast to the lungs from *Sox9^{CreERT2};Yap$^{f/f}$* mice (Fig. 1H,I; Fig. S1D,E).

Together, these data pointed to a compartment-specific role for Yap in the Sox9+ distal progenitors crucial to generate airways during early lung morphogenesis. This role is no longer seen once Sox2+ airway progenitors are established. Thus, the aberrant lung morphogenesis phenotype common to both *Shh^{Cre};Yap$^{f/f}$* and *Sox9^{CreERT2};Yap$^{f/f}$* mutants reflects the effect of Yap deficiency specifically in distal epithelial progenitors rather than in all epithelial cells along the proximal-distal axis of the lung.

Nuclear Yap prevents the aberrant cystic phenotype in Yap-deficient lungs *in vivo*

We further reasoned that, if Yap activity in emerging distal buds was crucial for lung patterning, then the severe disruption of airway morphogenesis seen in Yap-null mice could be corrected by providing nuclear Yap to epithelial progenitors from the earliest stages of lung development. To address this hypothesis, we used a *Rosa26*-driven human Yap allele (*R26Yap^{5SA}*), wherein all serines, normally targeted for Hippo phosphorylation, were mutated to alanines, preventing Yap cytoplasmic sequestration (Cotton et al., 2017). By crossing these mice into *Shh^{Cre};Yap$^{f/f}$* lines, we could then examine both the effect of replacing endogenous Yap with a constitutively expressed nuclear Yap (*Shh^{Cre};Yap$^{f/f}$;R26Yap^{5SA}*) and the effect of expressing nuclear Yap in the presence of one endogenous Yap allele as a gain-of-function model (*Shh^{Cre};Yap$^{f/+}$;R26Yap^{5SA}*). *Shh^{Cre};Yap$^{f/+}$* mice reached adulthood and were fertile, as shown in previous reports (Lin et al., 2017; Mahoney et al., 2014).

Gross analysis of E13.5-18.5 *Shh^{Cre};Yap$^{f/f}$;R26Yap^{5SA}* embryos revealed overall morphologically normal lungs with all lobes distinctly formed with none of the highly hypoplastic features or dilated cyst-like structures of the Yap-deficient animals (Fig. 2A-C; Figs S2 and S3B). *Yap^{5SA}*-expressing mutants undergoing branching morphogenesis showed nuclear Yap signals on nearly all epithelial cells in both Sox9+ and Sox2+ domains (Fig. S2B,D). Notably, nuclear signals were strong at the transition between distal buds and nascent airways at E13.5 and E15.5 (Fig. S2B,D, insets), suggesting that, in the presence of local nuclear Yap, Sox2+ airway progenitors were specified in the absence of endogenous Yap (Fig. S2B,D). Crucially, a cytoplasmic Yap signal was undetectable in *Shh^{Cre};Yap$^{f/f}$;R26Yap^{5SA}* lungs (Fig. 2D,E), demonstrating that endogenous Yap had been efficiently deleted and replaced by R26Yap^{5SA}. By E18.5, *Shh^{Cre};Yap$^{f/f}$;R26Yap^{5SA}* whole embryos were smaller (20.3 mm±1.21; P=0.0158) compared with *Yap$^{f/f}$;R26Yap^{5SA}* controls (23.3 mm±1.27), and could be readily distinguished by external abnormalities, such as a hunched posture, proximally bent thick limbs and a short tail (Fig. S3A,C). Although mutant lungs were also smaller (5.03 mm±0.41; P=0.0051) compared with controls (6.12 mm±0.62), when normalized by the respective whole-body length, the difference became statistically nonsignificant (Fig. S3B,C). IF of phosphorylated Yap (pYap) and Yap confirmed the expected subcellular distribution of signals in control and mutant lungs, and Hematoxylin and Eosin (H&E) staining showed distinct generations of airways and well-formed distal saccules in E18.5 *Shh^{Cre};Yap$^{f/f}$;R26Yap^{5SA}* lungs, compatible with efficient rescue of lung morphogenesis (Fig. 2G,H).

To further investigate a dose-dependent effect, we analyzed the lungs from *Shh^{Cre};Yap$^{f/+}$;R26Yap^{5SA}* mice, which carry an endogenous Yap allele in addition to the *Rosa26*-driven Yap^{5SA} construct. Overall morphological features of these lungs were similar to those of *Shh^{Cre};Yap$^{f/f}$;R26Yap^{5SA}* lungs without evidence of disruption of branching morphogenesis or sacculation (Fig. 2C,I), despite the persistence of one endogenous Yap allele, as visualized by faint cytoplasmic Yap stain (Fig. 2F). Thus, although loss of Yap has a profound impact on lung morphogenesis, constitutive expression has no obvious consequences for morphogenesis.

Dynamic patterns of Yap subcellular localization during distal tubule-to-saccule transition

Branching morphogenesis has been traditionally associated with the pseudoglandular stage of lung development (E11-E16), although there is recent evidence that this process extends to the late canalicular stage (~E17; Alanis et al., 2014). Our previous analysis of Yap expression in the lung focused on earlier stages (E12.5-E14.5; Mahoney et al., 2014). Thus, we expanded this study to later developmental stages using a similar IF protocol and Yap antibodies, which ensured high-resolution analysis of subcellular localization without the artifacts often seen when using signal amplification procedures.

Development (2019) 146, dev175810. doi:10.1242/dev.175810

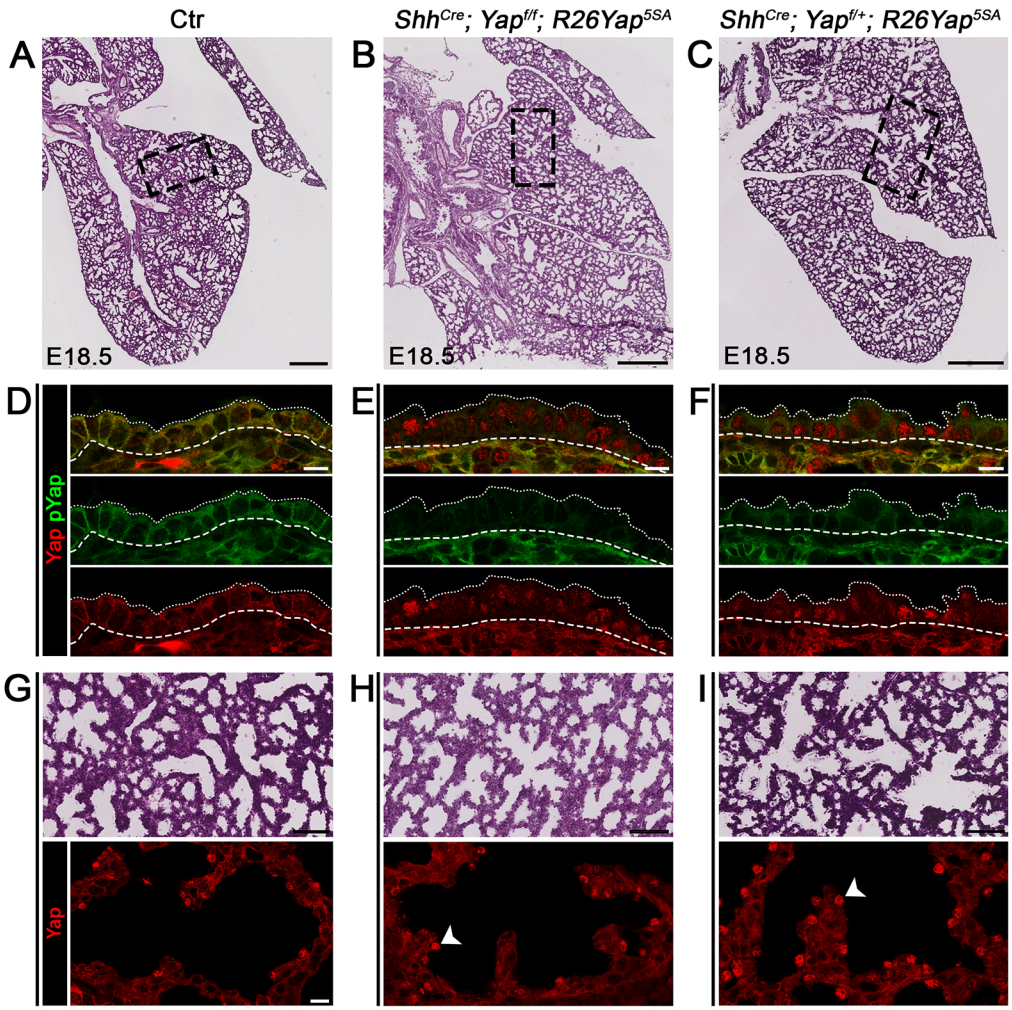

Fig. 2. Expression of nuclear Yap rescues the branching and sacculation defects of Yap-deficient lungs *in vivo*. (A-C) H&E staining in E18.5 control (Ctr) (A), *Shh*^{Cre};*Yap*$^{f/f}$;*R26Yap*^{5SA} (B) and *Shh*^{Cre};*Yap*$^{f/+}$;*R26Yap*^{5SA} (C). Multiple generations of airways and well-formed distal saccules in Yap deleted as in Ctr lungs are suggestive of the efficient rescue of lung morphogenesis by *Yap*^{5SA}. (D-F) Yap and pYap IF in airways of E18.5 lungs; (D) in Ctr lungs, there is a strong cytoplasmic signal (pYap) but very weak nuclear signal. (E) In *Shh*^{Cre};*Yap*$^{f/f}$;*R26Yap*^{5SA} lungs, there is no endogenous Yap signal but strong nuclear Yap signals in the epithelium. (F) In *Shh*^{Cre};*Yap*$^{f/+}$;*R26Yap*^{5SA} lungs, there are both cytoplasmic and nuclear Yap epithelial signals. Note strong nuclear signals in E and F but not in D, suggesting that the former signals represent *Yap*^{5SA} transgenes. Epithelial pYap is weaker in F (*Shh*^{Cre};*Yap*$^{f/+}$) than in D (Ctr), but mesenchymal Yap signals are similar in both, consistent with targeting strategy. Dashed and dotted lines in D-F outline the basement membrane and luminal aspect of the epithelium, respectively. (G-I) H&E and Yap IF showing the morphology and distribution of nuclear Yap signals in alveolar saccules of *Shh*^{Cre};*Yap*$^{f/f}$;*R26Yap*^{5SA} (H) and *Shh*^{Cre};*Yap*$^{f/+}$;*R26Yap*^{5SA} lungs (I), similar to Ctr (G; arrowheads indicate *Yap*^{5SA} transgenes). DAPI appears gray in all panels. Scale bars: 500 µm in A-C; 10 µm in D-F; 100 µm top and 10 µm (bottom) in G-I.

Analysis of E14.5 lungs confirmed the preferentially nuclear Yap localization in nascent Sox9+ distal buds (Fig. 3A). However, at E15.5, cytoplasmic signals became increasingly more noticeable, leading to an overall pancellular Yap staining at the bud tips and neighboring epithelium (Fig. 3B). Interestingly, by the end of the canalicular stage and onset of sacculation (E17-E17.5), the population of Sox9+ distal buds maintained strong Yap cytoplasmic signals but nearly ceased to express nuclear Yap (Fig. 3C). The presence of a strong LPCAT1 signal suggested that these cells were destined to become alveolar type 2 (AT2) cells (Fig. 3D). The immediately proximal Sox2-negative region still expressing pancellular Yap colocalized broadly with Hopx, suggesting that these cells initiate a program of alveolar type 1 (AT1) cell differentiation (Fig. 3E).

Recent studies implicated the appearance of protruding cells in distal buds undergoing sacculation as a mechanism that prevents protruded cells from flattening, thereby precipitating their differentiation into AT2 cells. We investigated the dynamic changes in Yap subcellular localization during these events in *Shh*^{Cre};*Rosa26*^{mTmG} mice. IF of GFP, Yap and Pro-SPC in lung sections of these mutants allowed prompt visualization of cell membranes and changes in cell shape in distal progenitors. TMX was administered (50 µg/g) at E15.5 and lungs were examined at E17-E17.5.

Sequential analysis of protrusions in distal epithelial tubules in E17-E17.5 lungs showed the nonoverlapping pattern of Pro-SPC/non-Yap-expressing cells (prospective AT2 cells) and the Pro-SPC-negative/Yap-expressing cells (Fig. S4A). As the lumen of the regions proximal to these protrusions enlarged, nuclear Yap+ cells appeared to flatten, whereas Yap-negative Pro-SPC-expressing cells that maintained minimal contact with the luminal surface retained their cuboidal shape (Fig. S4B,C). These patterns persisted in the E18.5 distal lungs (Fig. 4A; Figs S4 and S5), where IF-confocal imaging revealed cells expressing nuclear or pancellular Yap

Development (2019) 146, dev175810. doi:10.1242/dev.175810

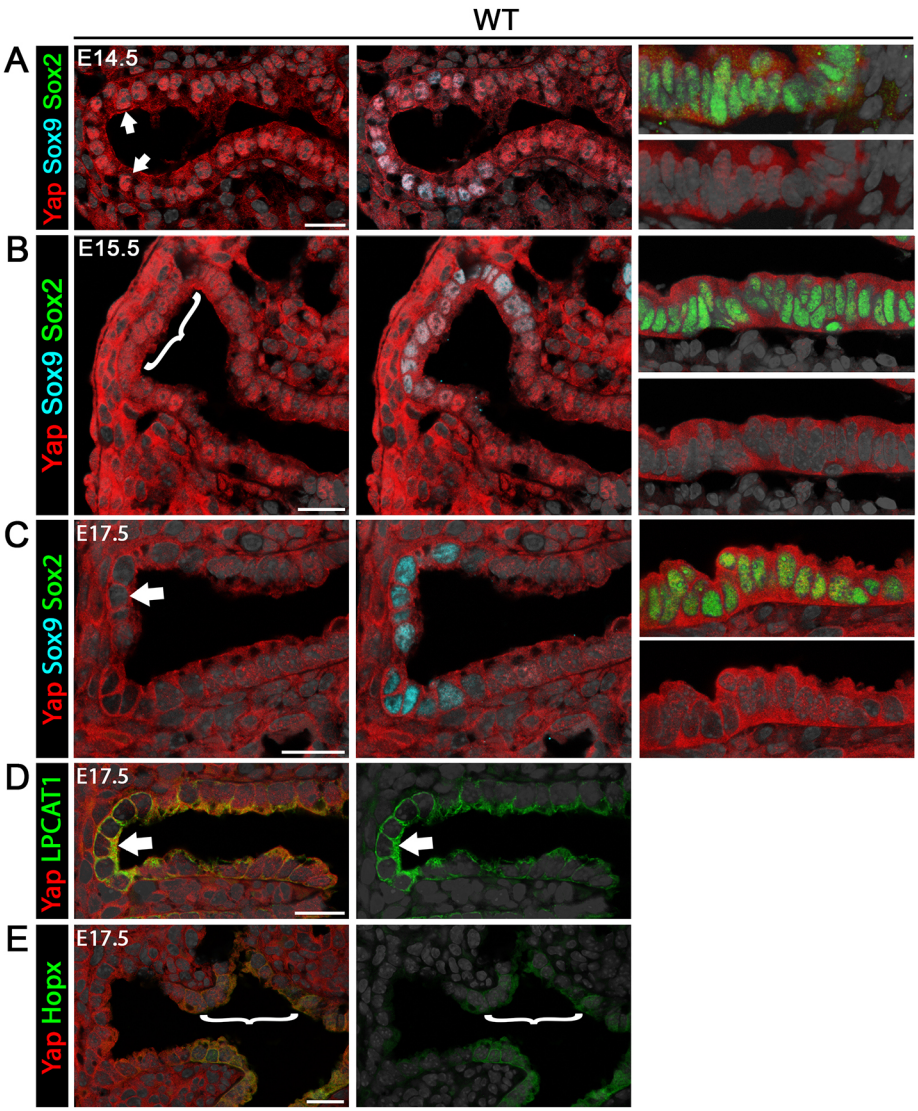

Fig. 3. Yap undergoes dynamic changes in subcellular localization in distal buds at the onset of sacculation. (A-C) IF for Yap, Sox9 and Sox2 in wild-type (WT) lungs showing dynamic stage-related changes in Yap subcellular localization from mostly nuclear (A: arrows, E14.5 left and middle panels), then pancellular (B: bracket, E15.5 left and middle panels) to cytoplasmic (C: arrow, E17.5 left and middle panels) in Sox9 progenitors. Yap stays largely cytoplasmic in Sox2+ airway epithelial cells regardless of stage (right panels). (D,E) IF in E17.5 lungs: LPCAT1 and cytoplasmic Yap overlap in distal buds (arrow), whereas Hopx appears more proximally where Yap is mostly pancellular (bracket). DAPI appears gray in all panels. Scale bars: 20 µm.

double-labeled with AT1 markers (T1a, Ager and Hopx) (Fig. 4A; Fig. S5, control). By contrast, Yap-negative cells consistently expressed markers of AT2 cells (Abca3, Pro-SPC, SPB and LPCAT1) (Fig. 4A; Fig. S5, control).

Nucleocytoplasmic shuttling is dispensable for distal differentiation and sacculation in the presence of nuclear Yap

These intriguing patterns led us to examine, first, how local Yap affected specifically these distal events during late development regardless of its subcellular localization. Our analysis of $Sox9^{CreERT2};Yap^{f/f}$ mice showed that, despite its aberrant, cyst-like appearance, the early identity of the distal epithelium (Sox9, Pro-SPC and Bmp4) was unaffected (Fig. S1A). However, it was unclear whether the progenitors in these cysts were still able to properly respond to signaling cues for late differentiation. Remarkably, despite the highly distorted morphology of distal airspaces, E18.5 $Sox9^{CreERT2};Yap^{f/f}$ lungs were extensively populated by AT2 cells, as demonstrated by the large number of cuboidal cells expressing multiple AT2 markers (Pro-SPC, SPB, LPCAT1 and Abca3; Fig. 4A; Fig. S5). By contrast, at late gestation, Yap-deficient Sox9 progenitors in these cysts were unable to turn on the AT1 markers T1a, Ager or Hopx (Fig. 4A; Fig. S5). Quantitative analysis confirmed the significant decrease in the percentage of AT1 and increase in the AT2 cell population (P=0.00169; Fig. 4B). We concluded that, although dispensable for AT2 cells, Yap is crucial for initiation of the program of AT1 cell differentiation.

Next, we examined how preventing the dynamic changes in Yap subcellular localization observed before sacculation would interfere with late distal differentiation. What if Yap was available but unable to undergo nucleocytoplasmic shuttling? The overall rescue of branching morphogenesis and sacculation of our $Shh^{Cre};Yap^{f/f};R26Yap^{5SA}$ mutants in the absence of Yap nucleocytoplasmic shuttling provided an opportunity to address this question. Analysis of E18.5 mutant lungs showed nuclear Yap in both AT1 and AT2 cells, in contrast to control ($Yap^{f/f};R26Yap^{5SA}$) littermates (nuclear Yap was only seen in AT1 cells) (Fig. 4C). We asked whether the presence of nuclear Yap ($R26Yap^{5SA}$) in distal epithelial buds at the onset of AT1 versus AT2 differentiation and the inability of Yap to be sequestered to the cytoplasm influenced distal cell fate decisions. Morphometric analysis showed a slight decrease in the proportion of AT2 cells (42.1±2.3%; P=0.0321), but no significant change in that of AT1 cells (48.7±3.2%; P=0.965) in mutants (Fig. 4D). Interestingly, maintained nuclear Yap expression led to a significant increase in the fraction of double Pro-SPC+T1a+ cells (9.2±1%; P=0.00134; Fig. 4D,E) relative to controls (2.7±0.4%).

Development (2019) 146, dev175810. doi:10.1242/dev.175810

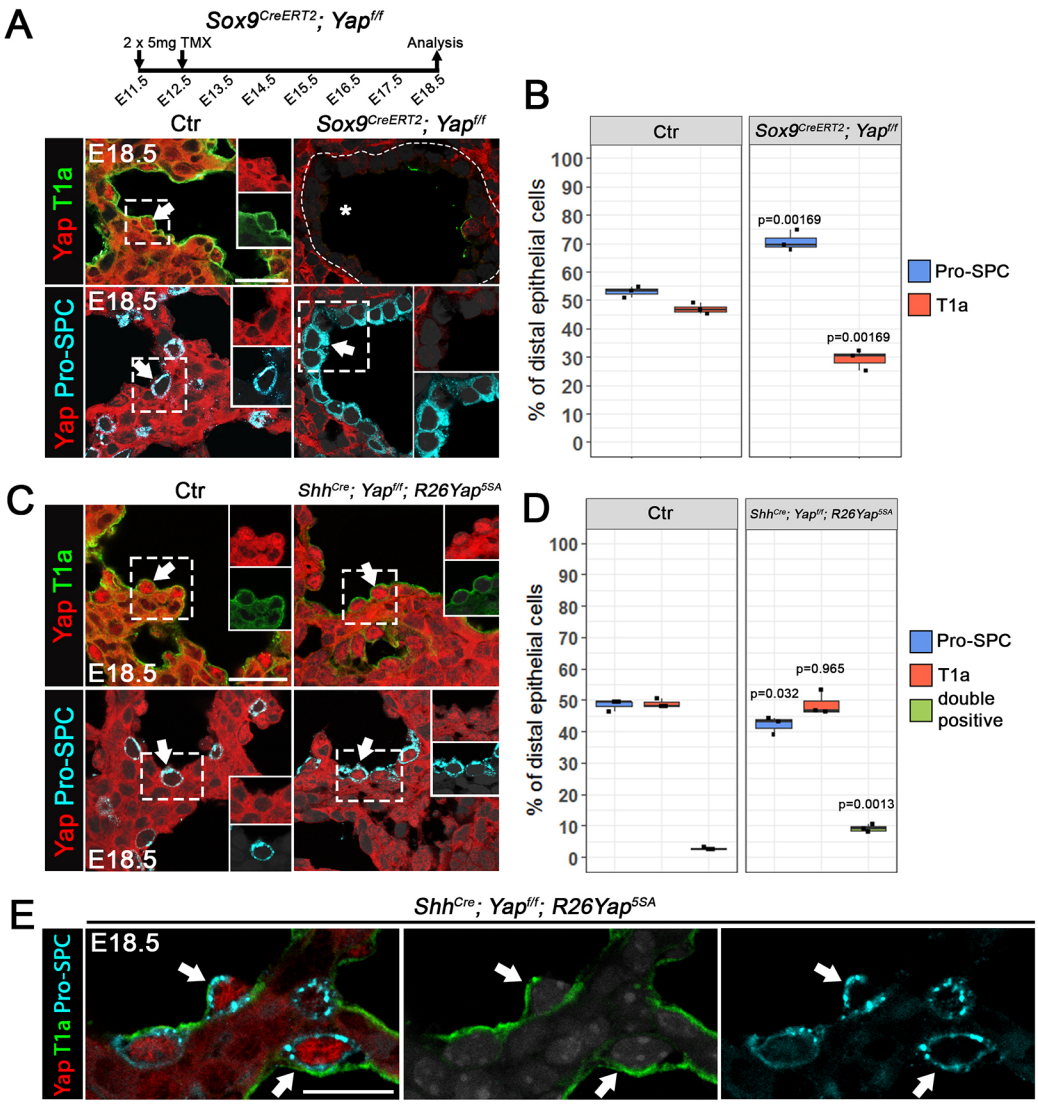

Fig. 4. Yap but not its nucleocytoplasmic shuttling is required for distal differentiation. (A-E) IF staining of Yap, T1a and Pro-SPC in E18.5 lungs from *Sox9*^{CreERT2}*;Yap*$^{f/f}$ [injected with 5 mg TMX at E11.5 and E12.5 (A)], *Shh*^{Cre}*;Yap*$^{f/f}$*;R26Yap*^{5SA} (C,E) and respective controls, imaged by confocal microscopy, and percentage of T1a+ and Pro-SPC+ cells, as representative of AT1 and AT2 cells, respectively, in the mutants indicated (B,D). Double T1a+ Pro-SPC+ cells in *Shh*^{Cre}*; Yap*$^{f/f}$*;R26Yap*^{5SA} depicted in E (arrows) and quantitated in D. Insets in A,C show single-channel images of boxed areas. Arrows in A,C indicate presence of the respective marker (T1a or pro-SPC). The disrupted differentiation of AT1 (asterisk in A) but not AT2 cells results in the unbalanced AT1/AT2 proportion in *Sox9*^{CreERT2}*; Yap*$^{f/f}$. By contrast, distal differentiation is only minimally affected by replacement of endogenous Yap with a transgene unable to undergo nucleocytoplasmic shuttling in *Shh*^{Cre}*;Yap*$^{f/f}$*;R26Yap*^{5SA}. *n*=3 lungs per genotype. *P*-values calculated using unpaired, two-tailed *t*-test. DAPI appears dark gray in all panels. Dashed lines denote the basement membrane (A). Scale bars: 20 µm. Boxplots represent the median (box, middle line), 1st and 3rd quartile (box, lower and upper limits, respectively), minimum and maximum (whiskers) and outliers (dots).

Thus, expression of Yap is crucial in distal progenitors to allow morphogenesis and differentiation of the distal lung; this function appears to be minimally affected by the inability of Yap to undergo nucleocytoplasmic shuttling.

Nucleocytoplasmic shuttling of Yap is crucial for integrity and differentiation of the developing airway epithelium

Yap has been shown to have a significant impact on airway epithelial differentiation of the adult lung, using both *in vivo* and *in vitro* methodologies (Lange et al., 2015; Lin et al., 2015; Mahoney et al., 2014; Otsubo et al., 2017; Szymaniak et al., 2015; Zhao et al., 2014). However, its role in the differentiation of developing airways remained elusive and could not be adequately concluded from the mouse genetic models reported. Difficulties included the severe arrest in airway morphogenesis with accumulated defects caused by early Yap inactivation in the embryonic lung, and efficiency of recombination in some of the mouse Cre lines reported (Lin et al., 2017).

The lack of morphogenetic abnormalities and preserved 3D structure of the airways of *Sox2*^{CreERT2}*;Yap*$^{f/f}$ mice provided an opportunity to explore this issue. E18.5 lungs from these mutants were examined by IF/confocal microscopy for the distribution and levels of epithelial markers of multiciliated and secretory cell differentiation. Both cell types were abundantly present in the airways of these mutants, although expression of CC10, which marks the secretory Club cells, was weaker. Quantitative analysis revealed a decrease in the proportion of CC10-expressing cells (P=0.0103), but an increase in that of the multiciliated cells [Foxj1: P=0.0154; acetylated alpha-tubulin (ac-aTub): P=0.00626] (Fig. 5A-D). These observations and the presence of

Development (2019) 146, dev175810. doi:10.1242/dev.175810

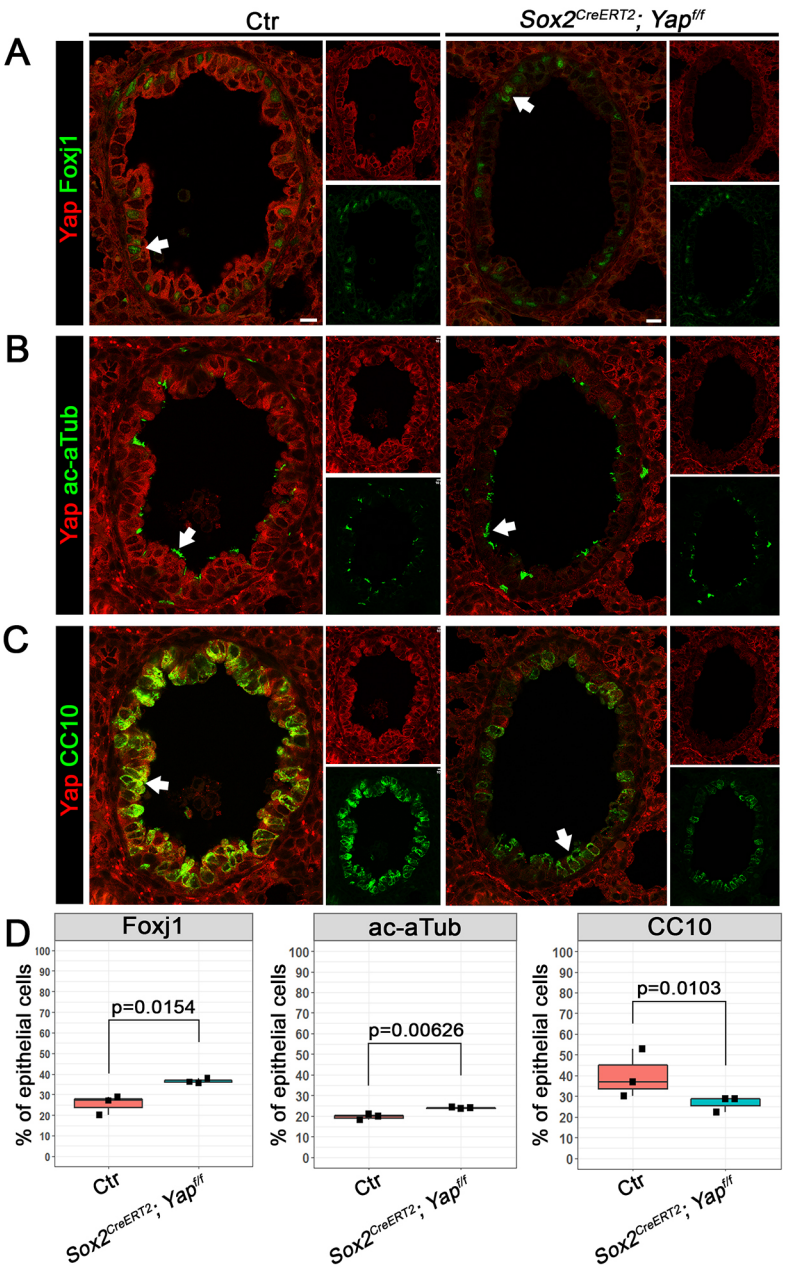

Fig. 5. Yap deletion in Sox2+ progenitors does not prevent airway differentiation and only leads to imbalance in airway cell types. (A-C) IF of Yap, Foxj1, ac-aTub and CC10 in intrapulmonary airways of E18.5 control and *Sox2*^{CreERT2}*;Yap*$^{f/f}$ lungs, injected with 5 mg TMX at E11.5, E13.5 and E15.5. Insets depict single channel images; arrows indicate representative signals used for quantitative analysis in (D). Decreased CC10 expression and percentage of secretory club cells and increase in multiciliated cells (Foxj1+, ac-aTub+). Boxplots represent the median (box, middle line), 1st and 3rd quartile (box, lower and upper limits, respectively), minimum and maximum (whiskers) and outliers (dots). *n*=3 lungs per genotype. *P*-values calculated using unpaired, two-tailed *t*-test. DAPI appears gray in all panels. Scale bars: 10 µm.

epithelial Yap largely in the cytoplasm of control airways suggested that, during development, Yap is unlikely to specify airway epithelial cell lineages. Instead, it could act in a mechanism influencing the differentiation of these cell types. Although not explored here, previous studies suggest a role for Yap in ciliogenesis and in the regulation of Notch, a known determinant of cell fate decisions in the airway epithelium (de Lima et al., 2016; Grampa et al., 2016; Kim et al., 2015; Mahoney et al., 2014; Totaro et al., 2017; Tschaharganeh et al., 2013; Tu et al., 2018; Yimlamai et al., 2014).

To gain additional insights into the role of Yap in developing airways, we investigated the lungs in which epithelial Yap was maintained constitutively active from the onset of lung development. Although Yap was clearly found in the cytoplasm of branching epithelial tubules, it was unclear whether cytoplasmic sequestration of Yap was required to carry its functions in developing airways**.** Thus, we examined the airways of *Shh*^{Cre}*;Yap*$^{f/f}$*;R26Yap*^{5SA} mice in which cytoplasmic Yap sequestration was abolished and Yap subsequently accumulated in the nucleus. Analysis of E18.5 mutants showed a highly disorganized epithelium in trachea, extrapulmonary bronchi and intrapulmonary airways (Fig. S6A,B). Although preserving its pseudostratified organization, multiple clumps of cells strongly labeled by nuclear Yap appeared in the lumen, detached from the airway epithelium. This phenotype was reminiscent of that reported in Lats1/2-null, Crb3-null and other mouse lines that result in Yap constitutive nuclear expression (Lange et al., 2015; Lin et al., 2015; Mahoney, 2014; Nantie et al., 2018; Otsubo et al., 2017; Szymaniak et al., 2015; Zhao et al., 2014). Interestingly, this hyperplastic phenotype was not associated with a significant increase in cell proliferation (Fig. S6D), because quantification of 5-ethynyl-2′-deoxyuridine (EdU)+ epithelial cells showed that EdU incorporation in *R26Yap*^{5SA}+ lungs was not significantly different from controls (*P*=0.317; Fig. S6D).

Development (2019) 146, dev175810. doi:10.1242/dev.175810

We asked whether the detached luminal cell clumps represented apoptotic cells, given that nuclear Yap has a role in anoikis (Zhao et al., 2012). IF analysis of Cleaved Caspase 3 (CC3) showed no evidence of apoptosis in the epithelium or in the detached clumps of cells (Fig. S6E). Intriguingly, the luminal clumps of detached cells that expressed strong nuclear Yap were also strongly labeled with T1a, suggestive of the AT1 fate (Fig. S6E). We asked whether these abnormalities could be exacerbated by an additional Yap allele in our gain-of-function model. Interestingly, airways from E18.5 *Shh^{Cre};Yap$^{f/+}$;R26Yap^{5SA}* lungs were very different from those of *Yap$^{f/f}$;R26Yap^{5SA}* controls but nearly indistinguishable from *Shh^{Cre};Yap$^{f/f}$;R26Yap^{5SA}* lungs (Fig. S6C). No significant difference in Edu incorporation was detected between control and *Shh^{Cre};Yap$^{f/+}$;R26Yap^{5SA}* lungs (P=0.608; Fig. S6D). Thus, we were unable to ascribe the appearance of the luminal clumps in mutant airways to excessive cell proliferation or cell death.

We then examined how the replacement of endogenous Yap with a constitutively active nuclear Yap, unable to shuttle to the cytoplasm from the earliest lung developmental stages, influenced airway epithelial differentiation. Confocal analysis of E18.5 *Shh^{Cre};Yap$^{f/f}$;R26Yap^{5SA}* lungs identified nuclear Yap at distinct levels (hereafter, Yap^{high}, Yap^{mid} or Yap^{low}) in the airway epithelium colocalizing with differentiation markers. The patterns of colocalization were determined for each marker and quantitated by Fluorescence Intensity Profile Analysis (see Materials and Methods; Fig. S7A-D). Yap^{high} cells did not colocalize with any of the markers tested, suggesting incompatibility with airway differentiation (Fig. 6A-D; Fig. S7E). In Yap^{mid} cells, only ~10-15% expressed Scgb3a2 or Foxj1, known as early markers of secretory and multiciliated cells, respectively (Fig. 6A,D; Fig. S7E). Surprisingly, CC10+ secretory cells colocalized with intermediate levels of nuclear Yap (35.6±4.2%; Fig. 6B,D). Although Scgb3a2 and CC10 are expressed in secretory cells, these markers did not appear to label the same cell population (Fig. S7F). p63+ basal cell precursors did not colocalize with Yap^{high}, although some did with Yap^{mid} (34±8.4%; Fig. 6C,D). Together, these data suggest that high levels of nuclear Yap abrogate airway lineage differentiation.

Maintained nuclear Yap activation alters the identity of airway progenitors during differentiation

Intriguingly, none of the major airway lineage markers was present in the cells efficiently expressing high levels of nuclear Yap (R26Yap^{5SA}). We asked whether, despite acquiring an airway fate earlier (Fig. S2), this fate was maintained with continued constitutive nuclear Yap expression. Thus, we stained E18.5 *Shh^{Cre};Yap$^{f/f}$;R26Yap^{5SA}* lungs with Sox2 and Yap and quantified the proportion of double-labeled cells in the different populations according to the intensity of the fluorescent Yap signals, as before. Surprisingly, only a few Sox2+ cells were seen in the Yap^{high} population (2.3±1.63%), whereas most Sox2+ cells expressed only weak nuclear Yap (Yap^{low}=74.1±5.9%) (Fig. 7A). This suggested that, overall, Yap^{high} cells could have lost their airway identity, reverting to an earlier distal progenitor state. This could explain the inability of these cells to turn on airway-specific programs of differentiation. Therefore, we stained these

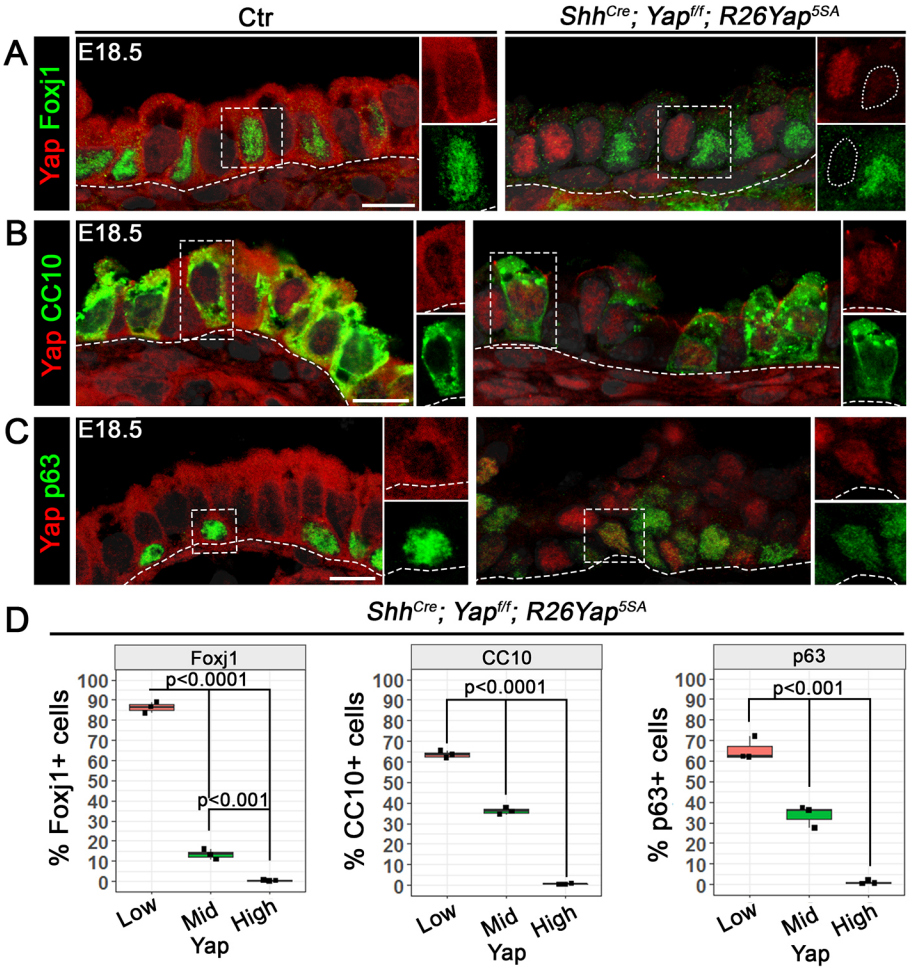

Fig. 6. Inability of *Yap^{5SA}* to undergo cytoplasmic localization is associated with severe disruption of airway epithelial differentiation. (A-C) Double IF of Yap with Foxj1 (A), CC10 (B) or p63 (C) in E18.5 control and *Shh^{Cre};Yap$^{f/f}$;R26Yap^{5SA}* lungs. (D) Percentage of cells labeled with each marker co-expressing low, mid and high levels of nuclear Yap as defined by signal intensity profile shown in Fig. S7A-C and represented as boxplots depicting the median (box, middle line), 1st and 3rd quartile (box, lower and upper lines, respectively) and minimum and maximum (whiskers). n=3 lungs per marker. None of these markers colocalize with Yap^{high} cells. P-values were calculated with one-way ANOVA followed by post-hoc Tukey test. DAPI appears gray in all panels. Dashed lines outline the basement membrane, dotted lines outline nuclei. Insets show single channel images of boxed areas. Scale bars: 20 µm.

Development (2019) 146, dev175810. doi:10.1242/dev.175810

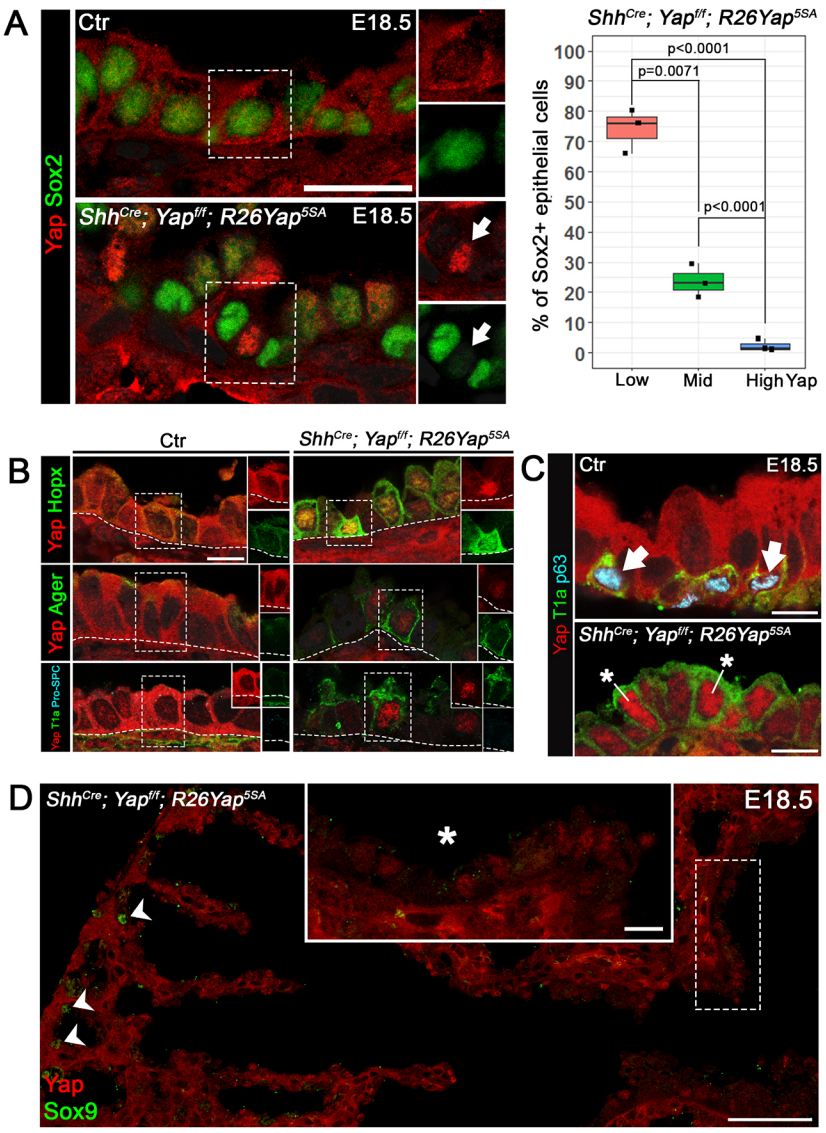

Fig. 7. Nucleocytoplasmic shuttling of Yap is required to maintain airway progenitor cell identity. (A) IF of Yap and Sox2 in E18.5 control and *Shh^{Cre};Yap$^{f/f}$;R26Yap^{5SA}* lungs (left). Arrows in insets highlight a Yap+/Sox2− cell. Percentage of Sox2+ cells co-expressing low, mid and high levels of nuclear Yap. Boxplots represent the median (box, middle line), 1st and 3rd quartiles (box, lower and upper lines, respectively) and minimum and maximum (whiskers). *n*=3 lungs per genotype. *P*-values were calculated with one-way ANOVA followed by post-hoc Tukey test. Very few nuclear Yap^{high} cells express Sox2. (B,C) IF staining of Yap with Hopx, Ager, T1a/Pro-SPC and p63 in E18.5 control and *Shh^{Cre};Yap$^{f/f}$;R26Yap^{5SA}* lungs. Nuclear Yap+ airway epithelial cells of *Shh^{Cre};Yap$^{f/f}$;R26Yap^{5SA}* express AT1 but not AT2 markers (B) and are not basal cells (C). Asterisks indicate the absence of p63 in the nucleus. (D) IF staining of Yap and Sox9 in E18.5 *Shh^{Cre};Yap$^{f/f}$;R26Yap^{5SA}* lungs. Nuclear Yap+ airway epithelial cells are Sox9 negative (inset, asterisk). Arrowheads indicate Sox9+ cells. DAPI appears gray in all panels. Dashed lines outline the basement membrane. Scale bars: 50 µm in D (overview); 20 µm in A,B; 10 µm in C,D (inset).

lungs with distal markers of early (Sox9 and Pro-SPC) and late (T1a, Hopx and Ager) cell fate. Although no Sox9 or Pro-SPC labeling was present, T1a, Hopx and Ager were strongly expressed in Yap^{high} airway epithelial cells in which Sox2 was inhibited (Fig. 7B,D; Fig. S7G), and T1a colocalized with Yap^{mid} airway cells (Fig. S7H). The nonoverlapping pattern of T1a with p63 ensured that the T1a-expressing Yap^{high} cells were not airway basal cells but indeed type 1 cells (Fig. 7C). Together, these data indicated that, although activation of transcriptional programs by nuclear Yap is essential for early morphogenesis, Yap nucleocytoplasmic shuttling is crucial in controlling these programs by bringing Yap preferentially to the cytoplasm in forming airways. This helps to consolidate proximal-distal fate in these compartments, allowing initiation of cell type-specific differentiation and ensuring that distal programs (such as the AT1 differentiation) do not occur in airways. These observations highlight the significance of the dynamic subcellular expression of Yap when airways are forming and during the transition from the canalicular to saccular stage reported here.

DISCUSSION

Here, we provide novel evidence of compartment-specific roles for Yap in lung morphogenesis and epithelial differentiation and how Yap subcellular localization influences these events. Lineage-tracing studies demonstrate that epithelial progenitors at the bud tips (Sox9+ and Id2+) are multipotent and leave the distal domain of branching tubules to give rise to all epithelial cell types of the airway and alveolar compartments (Rawlins et al., 2009; Yang et al., 2018). We found that, when Yap expression was disrupted selectively in Sox9+ progenitors of the developing lung, cells of the distal compartment were no longer able to respond to local cues to initiate a program of airway morphogenesis and ultimately form distal and proximal branches. Rather, *Sox9^{CreERT2};Yap$^{f/f}$* mice formed distal cystic structures, a phenotype essentially similar to that reported in *Shh^{Cre};Yap$^{f/f}$* mice and supported by studies in *Sox9^{Cre};Yap$^{f/f}$* mice (Lin et al., 2017), suggesting that the lung defect in *Shh^{Cre};Yap$^{f/f}$* mice results primarily from disruption of Yap-mediated events in Sox9+ progenitors. Remarkably, restoring Yap distal epithelial activity in a cell autonomous fashion and solely in the nucleus enabled cells to respond to these cues, allowing epithelial-mesenchymal cross talk for proper morphogenesis. Although our data suggest that Yap activity in distal progenitors is important for morphogenesis, we cannot rule out cell nonautonomous effects through altered epithelial-mesenchymal crosstalk, in the absence of a lineage tag. This is similarly true for our experiments wherein Yap was deleted in airway progenitors.

Development (2019) 146, dev175810. doi:10.1242/dev.175810

Under physiological conditions, nucleocytoplasmic shuttling of Yap is expected to occur in a dynamic fashion throughout all Yap-expressing cells of a developing structure. Nevertheless, several reports also show that, despite being continuously shuttled, the subcellular localization of Yap/Yorkie differs even within cell populations of the same organ, influenced by variables such as the stage in the cell cycle and others (Manning et al., 2018; Varelas, 2014). Indeed, previous reports demonstrated differences in Yap subcellular localization in the developing lung, preferentially nuclear in distal buds and cytoplasmic in forming airways (Mahoney et al., 2014; Szymaniak et al., 2015). However, less stringent staining protocols showing a rather pancellular distribution of Yap argued that any given region of the lung epithelium could be susceptible to loss of Yap and, thus, produce local branching defects (Lin et al., 2017). Here, we demonstrated that this is not the case, because no branching abnormalities were observed by deleting Yap in airway progenitors once Sox2 expression was established (Fig. 1E). Moreover, we provide new evidence of striking differences in Yap subcellular localization arising in the distal lung at the onset of sacculation. These dynamic patterns culminate with nuclear Yap-expressing cells differentiating into AT1 cells, in stark contrast to AT2 cells, in which Yap is largely cytoplasmic. Lastly, the distinct effects of nuclear Yap in *Shh*^{Cre};*Yap*$^{f/f}$;*R26Yap*^{5SA} mice rescuing Yap-dependent events in distal progenitors (branching and sacculation) but disturbing the integrity and differentiation of the airway epithelium, do not support the idea that proximal and distal compartments respond to Yap in the same fashion. This is consistent with our observation of distinct subcellular Yap localization in these compartments, rather than a model in which Yap is equally distributed in the nucleus and cytoplasm throughout the developing lung epithelium.

Remarkably, nuclear-cytoplasmic shuttling appears to be dispensable for all events associated with the distal lung, provided that nuclear Yap is available to mediate transcriptional events in distal progenitors. The steady-state levels of Yap expression driven by the *Rosa* locus in *Shh*^{Cre};*Yap*$^{f/f}$;*R26Yap*^{5SA} mice from the earliest developmental stages were sufficient to rescue the Yap-dependent signaling of all key events of the developing lung, including branching morphogenesis, sacculation and epithelial differentiation. Thus, expression of a Hippo-independent Yap can substitute for endogenous Yap and exert its function in the distal lung.

It was surprising that in our gain-of-function *Shh*^{Cre};*Yap*$^{f/+}$;*R26Yap*^{5SA} model, the activity of an additional Yap allele had no notable increased effect in any of the lung compartments compared with the *Shh*^{Cre};*Yap*$^{f/f}$;*R26Yap*^{5SA} model. We reasoned that the abnormal ectopic AT1 and disruption of the airway epithelial integrity in these mutants was probably a function of the continued expression of Yap in the nucleus rather than an increase in Yap dosage. This is also consistent with observations from other genetic models in which Hippo components and effectors, such as Mst1/2 (Lange et al., 2015; Lin et al., 2015), Last1/2 (Nantie et al., 2018) and Crb3 (Szymaniak et al., 2015), were inactivated.

Notably, in the absence of nucleocytoplasmic shuttling, constitutively active nuclear Yap inhibited airway progenitor cell identity, as demonstrated by the low Sox2 expression in high Yap-expressing cells. Indeed, Yap regulation of Sox2 expression has been previously reported and further confirmed in the present work by chromatin immunoprecipitation (ChIP) analysis in Sox2-expressing airway progenitors (Mahoney et al., 2014; Fig. S7I). Interestingly, neither bud morphogenesis nor initiation of the patterning events that give rise to airways was disrupted in these mutants despite the maintained expression of nuclear Yap and lack of cytoplasmic Yap. Moreover, our analysis of *Shh*^{Cre};*Yap*$^{f/f}$;*R26Yap*^{5SA} and *Shh*^{Cre};*Yap*$^{f/+}$;*R26Yap*^{5SA} mice showed that the differentiation program of the distal lung epithelium was remarkably resistant to the maintained expression of constitutively active Yap. This did not prevent AT2 cells from forming and had only a relatively mild effect on the balance of AT1×AT2 distal cells, unlike a previous study, which showed an increase in the number of AT1 at the cost of AT2 cells (Nantie et al., 2018). The difference in findings could be explained by the distinct genetic model used. Whereas we had Yap^{5SA} under the control of the *Rosa26* locus, Nantie et al. used a doxycycline-inducible *Sftpc* promoter construct, which drives high levels of Yap^{S127A} expression throughout lung development. This could have allowed a more rapid and efficient accumulation of Yap^{S127A}, leading to a severe disruption of the balance of AT1×AT2 cells. Nevertheless, both studies observed ectopic AT1 cells in airways as a result of forced nuclear Yap, suggesting that Yap is involved in the differentiation of AT1 cells.

Together, these findings emphasize the requirement of a mechanism of nucleocytoplasmic shuttling to foster Yap cytoplasmic sequestration in nascent airway epithelial progenitors. This would consolidate the proximal fate, allow compartment-specific initiation of cellular differentiation and maintain integrity of the architecture of the pseudostratified epithelium.

MATERIALS AND METHODS

Mouse lines

All studies were approved by the Columbia University Irving Medical Center Institutional Animal Care and Use Committee (IACUC). *Shh*^{Cre} (Harfe et al., 2004), *Sox9*^{CreERT2} (Soeda et al., 2010), *Sox2*^{CreERT2} (Arnold et al., 2011), *Yap*$^{f/f}$ (Camargo et al., 2007), *R26Yap*^{5SA} (Cotton et al., 2017) and *Rosa26*^{mTmG} (Muzumdar et al., 2007) lines have been described previously. To disrupt Yap specifically in the developing distal or airway epithelial compartments, *Sox9*^{CreERT2} and *Sox2*^{CreERT2} lines were crossed with *Yap*$^{f/f}$ lines. To generate mice in which endogenous Yap was replaced by constitutively active nuclear Yap, *Shh*^{Cre};*Yap*$^{f/+}$ lines were crossed with *R26Yap*^{5SA} mutants. TMX (Sigma, T5648) was dissolved in sunflower seed oil (Sigma, S5007) at a stock concentration of 20 mg/ml. The various TMX-administration regimens are described in the results section. Detection of a vaginal plug was considered to be E0.5. All mouse lines were generated in a B6/C57 background, except the *R26Yap*^{5SA} line (originally CD1). *Sox9*^{CreERT2} and *Sox2*^{CreERT2} lines were a gift from Dr Jianwen Que (Columbia University Irving Medical Center), the *Yap*$^{f/f}$ line from Dr Fernando Camargo (Harvard University) and the *R26Yap*^{5SA} line was from Dr Junhao Mao (University of Massachusetts). For crosses that involved the *Shh*^{Cre} allele, matings were set up such that only the male was to carry this allele. For other matings, there was no preference in bearer of the Cre construct.

Histology and immunofluorescent staining

Embryonic lungs at the developmental stages indicated were dissected, rinsed in PBS and fixed in 4% paraformaldehyde in PBS overnight at 4°C. Samples were then processed for frozen (optimal cutting temperature; OCT) embedding. H&E staining was performed by the Columbia University Irving Medical Center, Herbert Irving Comprehensive Cancer Center Molecular Pathology (histology) core, and imaged by Leica SCN400 Slide Scanner. Immunofluorescent staining was performed on 5-8-µm-thick tissue sections. Slides were subjected to heat-based antigen retrieval using a citrate-based buffer (Vector Labs, H-3300) for 8:30 min and blocked at room temperature (RT) for 1 h in 5% donkey serum in PBS. Staining with mouse primary antibodies was performed using MOM kit (Vector Labs, BMK-2202). Sections were incubated overnight with primary antibodies at 4°C. The following day, slides were washed, incubated for 2 h with Alexa Fluor-conjugated secondary antibodies as well as NucBlue Fixed Cell Stain ReadyProbes (DAPI) (Invitrogen, R37606) diluted in 5% donkey serum, washed again and finally mounted using

Development (2019) 146, dev175810. doi:10.1242/dev.175810

Prolong Gold anti-fade (Invitrogen, P36930) reagent and imaged on a Leica DMi-8 Deconvolution microscope, and a Zeiss LSM 710 confocal microscope system.

The following primary antibodies were used: rabbit anti-Abca3 (1:1000, Seven Hills, WRAB-70565), rabbit anti-acetylated α-tubulin (1:3000, Cell Signaling, 5335S), mouse anti-acetylated α-tubulin (1:3000, Sigma, T7451), rabbit anti-Ager (1:100, AbCam, ab3611), goat anti-CC10 (1:100, Santa Cruz, sc-9772), rabbit anti-cleaved caspase 3 (1:100, Cell Signaling, 9661P), mouse anti-FoxJ1 (1:100, eBioscience, 14-9965-82), rabbit anti-Hopx (1:100, Santa Cruz, SC-30216), rabbit anti-Nkx2.1 (1:1000, Seven Hills, WRAB-TTF1), rabbit anti-p63a (1:100, Cell Signaling, 13109S), rat anti-scgb3a2 (1:100, R&D Systems, MAB3465), rat anti-Sox2 (1:200, eBioscience, 14-9811-82), goat anti-Sox9 (1:200, R&D systems, AF3075), rabbit anti-pYap (1:50, Cell Signaling, 4911S), rabbit anti-Pro-SPC (1:1000, Seven Hills, WRAB-76694), hamster anti-T1a (1:50, Developmental Studies Hybridoma Bank #8.1.1, RRID: AB_531893), rabbit anti-Yap (1:100, Cell Signaling, 14074S) and mouse anti-Yap (1:100, Santa Cruz, sc-101199).

The following secondary antibodies were used: donkey anti-goat (conjugated with Alexa Fluor 568 or 647), goat anti-hamster (conjugated with Alexa Fluor 647), donkey anti-mouse (conjugated with Alexa Fluor 488, 568 or 647), donkey anti-rabbit (conjugated with Alexa Fluor 488, 568 or 647), donkey anti-rat (conjugated with Alexa Fluor 488 or 647) and donkey anti-chicken (conjugated with Alexa Fluor 488). All secondary antibodies were obtained from either Jackson ImmunoResearch or Fisher Scientific.

In situ hybridization

In situ hybridization was performed as described before (Chen et al., 2007). Briefly, probes were synthesized by PCR from mouse genomic cDNA. The primers (including T3 and T7 sequences) were as follows: forward primer: AATTAACCCTCACTAAAGGGAAGCTAGGTGAGTTCGGCA-TC; reverse primer: TAATACGACTCACTATAGGGGCTCCTAGCAGG-ACTTGGCAT. Frozen sections were subjected to heat-based antigen retrieval in a citrate-based buffer (Vector Labs, H-3300), acetylated, permeabilized in PBST and prehybridized in prehybridization buffer for 2 h. Hybridization with a *Bmp4* probe proceeded overnight at 72°C in a humidified chamber. The following day, slides were rinsed in SSC buffer, blocked in 2% sheep serum and incubated in anti-digoxigenin-AP Fab fragments (1:2500, Roche, 11093274910) overnight at 4°C. The next day, the slides were rinsed in PBST and developed in BM Purple AP Substrate (Roche, 11442074001). Slides were then imaged on a Leica DMi-8 Deconvolution microscope.

EdU incorporation assay

Cell proliferation was assessed in control and $R26Yap^{5SA}$-expressing $Shh^{Cre};Yap^{f/f}$ or $Shh^{Cre};Yap^{f/+}$ mice by exposing embryos *in utero* to 1 mg EdU via intraperitoneal injection in mothers at gestational day E17.5 (5 mg/ml stock solution in PBS). Embryos were harvested 24 h later and processed for OCT embedding and sectioning. EdU was detected by immunostaining using the Click-iT EdU Alexa Fluor 647 Imaging kit (Thermo Fisher Scientific, C10340) following antigen retrieval. Sections were subsequently co-stained for Yap as described above.

Yap transcriptional activity in airway progenitors

Yap recruitment and activation of transcription at the Sox2 locus was examined by ChIP-PCR in airway epithelial progenitors (basal cells) isolated from adult mouse trachea as described previously (Mahoney et al., 2014). Briefly, basal cells were expanded in submerged cell culture conditions for 5 days (You et al., 2002), then washed, fixed and sonicated, such that ∼200-bp DNA fragments were obtained. Samples were incubated with rabbit anti-Yap (Cell Signaling, 14074S) or IgG (Cell Signaling, 3600S) primary antibodies (2.5 µg/ml) overnight at 4°C. The next day, samples were incubated with Dynabeads Protein G Immunoprecipitation Kit (Invitrogen, 100.07D) for 2 h at 4°C and washed with NaCl overnight at 65°C. Following uncrossing of the DNA, DNA was purified using a Qiagen Qiaquick PCR purification kit (Qiagen, 28104). PCR of Sox2 was carried out on genomic DNA, ChIP input DNA and DNA pulled down by either Yap or IgG antibodies, using three primer sets: negative control (non-Yap-TEAD-binding site upstream of Sox2 locus), primer pair 1 (predicted Yap-TEAD-binding site in Sox2 promoter), and primer pair 2 (TEAD-binding sequence within Sox2-coding region) (Fig. S7I). Given that primer pair 2 spanned a region within the Sox2-coding region, no TEAD binding was expected and, therefore, only primer pair 1 was hypothesized to generate a band. The following primers were used: negative control forward primer: TCTGCTGTTGGCTTTCATTG; reverse primer: GGTAACCGT-TGTTGGGTTGT. Primer pair 1 forward primer: ATTGAGTTATCAAG-GCAGTA; reverse primer: GCAGTAATTAGCGAGAAGTA. Primer pair 2 forward primer: GTTGTCCACATCAACTCGTT; reverse primer: CGCCAGATAAGTGGGAGGTT.

Fetal breathing movements in lung explants

$Shh^{Cre};R26^{mTmG}$ embryos were dissected at E16.5 and transferred to a 60-mm dish coated with silica gel. The four limbs of each embryo were affixed to the silica gel using needles. Ribs and sternum were removed to expose the heart and lung. A 30-gauge needle was inserted into the right ventricle. DMEM/F12 medium supplemented with 30% FBS and 1 U/ml penicillin-streptomycin (Thermo Fisher Scientific) was pumped (BT100-2J, Longer) into the heart at the speed of 50-60 µl/min. To mimic fetal breathing movements, a 30-gauge needle was inserted into the trachea and PBS was pumped into and out of the trachea at a speed of 6-8 µl/10 s (each time). The frequency of these fetal breathing movements was 6 breaths/min.

Quantifications and statistical analysis

All image-based quantification analyses were performed in ImageJ (version 1.50i) (Schneider et al., 2012), using plugin BioFormats (Linkert et al., 2010). Statistical analysis was performed in Microsoft Excel 2016 or R (version 3.4.3, R Core Team, 2014), running in RStudio (version 1.1.383, RStudio, 2013), using R package ggplot2 (Wickam, 2016). For comparison of two groups, statistical significance was determined by a two-sample two-tailed *t*-test (Figs 4B and 5D). For comparison of three groups or more, a one-way ANOVA followed by a post-hoc Tukey test was used (Figs 4D, 6D, 7A; Figs S3C, S6D, S7E). N values can be found in figure legends and represent the number of animal samples used per genotype. Data in graphs are presented as a boxplot with median, minimum, 1st and 3rd quantiles, and the maximum value, as indicated in figure legends. Statistical significance was defined as $P<0.05$.

For the measurement of lung length of $R26Yap^{5SA}$+ litters, photographs were taken of the right lateral side of each embryo, as well as ventral photographs of the respective lungs. Body length (mm) was obtained from measurements using a ruler of the head-to-tail distance of the embryo. Lung length (mm) was obtained similarly by measuring the distance between the upper and lower edge (anterior-posterior axis) of the left lungs. Lung-to-body length ratios were calculated by dividing lung length by body length. For both full-body as well as lung lengths, control n=13, $Shh^{Cre};Yap^{f/f};R26Yap^{5SA}$ n=4 and $Shh^{Cre};Yap^{f/+};R26Yap^{5SA}$ n=8.

Quantification of the number of CC10+, FoxJ1+ or ac-aTub+ cells in E18.5 $Sox2^{CreERT2};Yap^{f/f}$ lungs was performed in three control and three mutant samples. Three nonconsecutive sections were stained per sample for each marker, after which the number of marker+ cells was counted. Cell counts were normalized per sample by dividing the number of marker+ cells by the total cell count to obtain a per sample percentage of marker+ cells contributing to the airway epithelium. Data were presented in boxplots (Fig. 5D).

To determine the proportion of epithelial cells expressing Yap in various cell types, nonconsecutive sections from E18.5 $Shh^{Cre};Yap^{f/f};R26Yap^{5SA}$ lungs (n=3) were co-stained with Yap and each of the following cell differentiation markers: T1a (alveolar type 1), Scgb3a2 (secretory), CC10 (secretory Club), p63 (pre-basal), FoxJ1 (early multiciliated) or Sox2 (airway progenitor). Nine sections were stained per marker deriving from three biological samples and photographed on a Leica DMi-8 deconvolution microscope. Despite being expressed from a *Rosa26* promoter, the intensity of Yap5SA signals varied among airway progenitors. Profile analysis of signal intensity across a line (in µm) was performed in representative areas of Yap double-labeled sections, using ImageJ macro RGB_Profile_Plot (Fig. S7A-D). The signal intensity range (0-255) of Yap was then

classified into three categories (0-85, 85-170 and 170-225), which were used to define low, intermediate (mid) and high Yap signal levels, respectively (Fig. S7A-D). Colocalization of the various markers with each of these Yap signal level categories was then quantified and represented as a percentage in graph form (Fig. 6D; Fig. S7E,H).

Quantification of proliferating cells was performed in three nonconsecutive sections of E18.5 control (n=3), $Shh^{Cre};Yap^{f/f};R26Yap^{5SA}$ (n=3) and $Shh^{Cre};Yap^{f/f};R26Yap^{5SA}$ (n=2) EdU-labeled sections. Confocal microscopy images were imported into ImageJ, Nkx2.1/Sox2 and EdU channels were colored red and green, respectively, and double-labeled cells (appearing yellow) were highlighted and counted by consecutively using the (color) threshold and particle analysis functions. The automated count of the cells was manually checked for accuracy. Values for each group were summed per sample to obtain average numbers of proliferating cells and presented as percentage of EdU+ epithelial cells and represented in boxplot graphs (Fig. S6D).

Quantification of the number of AT1 and AT2 cells in control, $Sox9^{CreERT2};Yap^{f/f}$ and $Shh^{Cre};Yap^{f/f};R26Yap^{5SA}$ lungs (n=3 per genotype) was performed in three nonconsecutive sections by staining for T1a, Pro-SPC and Yap followed by confocal microscopy to image up to ten nonoverlapping fields per section. The number of T1a+ and Pro-SPC+ cells was manually counted using the ImageJ Cell Counter until a total of ∼1000 cells was counted per section. The percentage of AT1 and AT2 cells was derived by dividing the number of counted cells by the total number of cells counted per section, after which the percentages were averaged per sample and represented in boxplot graphs (Fig. 4B,D).

Acknowledgements
We would like to thank Xaralabos Varelas, Munemasa Mori, Maria Stupnikov and Ying Yang for technical advice and thoughtful discussions, and Dr Jianwen Que and Dr Junhao Mao for generously providing the $Sox9^{CreERT2}$ and $Sox2^{CreERT2}$, and $R26Yap^{5SA}$ mouse lines, respectively.

Competing interests
The authors declare no competing or financial interests.

Author contributions
Conceptualization: B.J.v.S., W.V.C.; Methodology: B.J.v.S., J. Lu, J. Li, N.T., W.V.C.; Validation: B.J.v.S., J.Q., J. Lu, J. Li, N.T.; Formal analysis: B.J.v.S., J.Q., J. Lu, J. Li, N.T., W.V.C.; Investigation: B.J.v.S., J.Q., J. Li; Resources: J. Lu, N.T., W.V.C.; Data curation: N.T.; Writing - original draft: B.J.v.S., W.V.C.; Writing - review & editing: B.J.v.S., W.V.C.; Visualization: B.J.v.S., J.Q., J. Lu, J. Li, N.T.; Supervision: J. Lu, W.V.C.; Project administration: W.V.C.; Funding acquisition: N.T., W.V.C.

Funding
This work was supported by the National Institutes of Health [NIH-NHLBI R35-HL135834-01 to W.V.C.]; and National Key Research and Development Program of China [2017YFA0103501 to N.T.]. Deposited in PMC for release after 12 months.

Supplementary information
Supplementary information available online at http://dev.biologists.org/lookup/doi/10.1242/dev.175810.supplemental

References
Alanis, D. M., Chang, D. R., Akiyama, H., Krasnow, M. A. and Chen, J. (2014). Two nested developmental waves demarcate a compartment boundary in the mouse lung. *Nat. Commun.* **5**, 3923. doi:10.1038/ncomms4923

Arnold, K., Sarkar, A., Yram, M. A., Polo, J. M., Bronson, R., Sengupta, S., Seandel, M., Geijsen, N. and Hochedlinger, K. (2011). Sox2+ adult stem and progenitor cells are important for tissue regeneration and survival of mice. *Cell Stem Cell* **9**, 317-329. doi:10.1016/j.stem.2011.09.001

Camargo, F. D., Gokhale, S., Johnnidis, J. B., Fu, D., Bell, G. W., Jaenisch, R. and Brummelkamp, T. R. (2007). YAP1 Increases organ size and expands undifferentiated progenitor Cells. *Curr. Biol.* **17**, 2054-2060. doi:10.1016/j.cub.2007.10.039

Chen, F., Desai, T. J., Qian, J., Niederreither, K., Lü, J. and Cardoso, W. V. (2007). Inhibition of Tgf beta signaling by endogenous retinoic acid is essential for primary lung bud induction. *Development* **134**, 2969-2979. doi:10.1242/dev.006221

Cotton, J. L., Li, Q., Ma, L., Park, J.-S., Wang, J., Ou, J., Zhu, L. J., Ip, Y. T., Johnson, R. L. and Mao, J. (2017). YAP/TAZ and hedgehog coordinate growth and patterning in gastrointestinal mesenchyme. *Dev. Cell* **43**, 35-47.e4. doi:10.1016/j.devcel.2017.08.019

de Lima, J. E., Bonnin, M. A., Birchmeier, C. and Duprez, D. (2016). Muscle contraction is required to maintain the pool of muscle progenitors via yap and notch during fetal myogenesis. *Elife* **5**, 1-25. doi:10.7554/elife.15593

Grampa, V., Delous, M., Zaidan, M., Odye, G., Thomas, S., Elkhartoufi, N., Filhol, E., Niel, O., Silbermann, F., Lebreton, C. et al. (2016). Novel NEK8 mutations cause severe syndromic renal cystic dysplasia through YAP dysregulation. *PLoS Genet.* **12**, 1-32. doi:10.1371/journal.pgen.1005894

Harfe, B. D., Scherz, P. J., Nissim, S., Tian, H., McMahon, A. P. and Tabin, C. J. (2004). Evidence for an expansion-based temporal Shh gradient in specifying vertebrate digit identities. *Cell* **118**, 517-528. doi:10.1016/j.cell.2004.07.024

Kim, J., Jo, H., Hong, H., Kim, M. H., Kim, J. M., Lee, J.-K., Heo, W. D. and Kim, J. (2015). Actin remodelling factors control ciliogenesis by regulating YAP/TAZ activity and vesicle trafficking. *Nat. Commun.* **6**, 6781. doi:10.1038/ncomms7781

Lange, A. W., Sridharan, A., Xu, Y., Stripp, B. R., Perl, A.-K. and Whitsett, J. A. (2015). Hippo/Yap signaling controls epithelial progenitor cell proliferation and differentiation in the embryonic and adult lung. *J. Mol. Cell Biol.* **7**, 35-47. doi:10.1093/jmcb/mju046

Lin, C., Yao, E. and Chuang, P.-T. (2015). A conserved MST1/2-YAP axis mediates Hippo signaling during lung growth. *Dev. Biol.* **4**, 1-13. doi:10.3390/jdb4010001

Lin, C., Yao, E., Zhang, K., Jiang, X., Croll, S., Thompson-Peer, K. and Chuang, P.-T. (2017). YAP is essential for mechanical force production and epithelial cell proliferation during lung branching morphogenesis. *Elife* **6**, 1-25. doi:10.7554/eLife.21130

Linkert, M., Rueden, C. T., Allan, C., Burel, J.-M., Moore, W., Patterson, A., Loranger, B., Moore, J., Neves, C., MacDonald, D. et al. (2010). Metadata matters: access to image data in the real world. *J. Cell Biol.* **189**, 777-782. doi:10.1083/jcb.201004104

Liu, Z., Wu, H., Jiang, K., Wang, Y., Zhang, W., Chu, Q., Li, J., Huang, H., Cai, T., Ji, H. et al. (2016). MAPK-mediated YAP activation controls mechanical-tension-induced pulmonary alveolar regeneration. *Cell Rep.* **16**, 1810-1819. doi:10.1016/j.celrep.2016.07.020

Mahoney, J. E., Mori, M., Szymaniak, A. D., Varelas, X. and Cardoso, W. V. (2014). The hippo pathway effector yap controls patterning and differentiation of airway epithelial progenitors. *Dev. Cell* **30**, 137-150. doi:10.1016/j.devcel.2014.06.003

Manning, S. A., Dent, L. G., Kondo, S., Zhao, Z. W., Plachta, N. and Harvey, K. F. (2018). Dynamic fluctuations in subcellular localization of the hippo pathway effector yorkie in vivo. *Curr. Biol.* **28**, 1651-1660.e4. doi:10.1016/j.cub.2018.04.018

Mauviel, A., Nallet-Staub, F. and Varelas, X. (2012). Integrating developmental signals: a Hippo in the (path)way. *Oncogene* **31**, 1743-1756. doi:10.1038/onc.2011.363

Muzumdar, M. D., Tasic, B., Miyamichi, K., Li, L. and Luo, L. (2007). A global double-fluorescent Cre reporter mouse. *Genesis* **45**, 593-605. doi:10.1002/dvg.20335

Nantie, L. B., Young, R. E., Paltzer, W. G., Zhang, Y., Johnson, R. L., Verheyden, J. M. and Sun, X. (2018). *Lats1/2* inactivation reveals Hippo function in alveolar type I cell differentiation during lung transition to air breathing. *Development* **145**, dev163105. doi:10.1242/dev.163105

Otsubo, K., Goto, H., Nishio, M., Kawamura, K., Yanagi, S., Nishie, W., Sasaki, T., Maehama, T., Nishina, H., Mimori, K. et al. (2017). MOB1-YAP1/TAZ-NKX2.1 axis controls bronchioalveolar cell differentiation, adhesion and tumour formation. *Oncogene* **36**, 4201-4211. doi:10.1038/onc.2017.58

Que, J., Luo, X., Schwartz, R. J. and Hogan, B. L. M. (2009). Multiple roles for Sox2 in the developing and adult mouse trachea. *Development* **136**, 1899-1907. doi:10.1242/dev.034629

Rawlins, E. L., Clark, C. P., Xue, Y. and Hogan, B. L. M. (2009). The Id2+ distal tip lung epithelium contains individual multipotent embryonic progenitor cells. *Development* **136**, 3741-3745. doi:10.1242/dev.037317

Schneider, C. A., Rasband, W. S. and Eliceiri, K. W. (2012). NIH Image to ImageJ: 25 years of image analysis. *Nat. Method.* **9**, 671-675. doi:10.1038/nmeth.2089

Soeda, T., Deng, J. M., De Crombrugghe, B., Behringer, R. R., Nakamura, T. and Akiyama, H. (2010). Sox9-expressing precursors are the cellular origin of the cruciate ligament of the knee joint and the limb tendons. *Genesis* **48**, 635-644. doi:10.1002/dvg.20667

Szymaniak, A. D., Mahoney, J. E., Cardoso, W. V. and Varelas, X. (2015). Crumbs3-mediated polarity directs airway epithelial cell fate through the hippo pathway effector yap. *Dev. Cell* **34**, 283-296. doi:10.1016/j.devcel.2015.06.020

Totaro, A., Castellan, M., Battilana, G., Zanconato, F., Azzolin, L., Giulitti, S., Cordenonsi, M. and Piccolo, S. (2017). YAP/TAZ link cell mechanics to Notch signalling to control epidermal stem cell fate. *Nat. Commun.* **8**, 15206. doi:10.1038/ncomms15206

Tschaharganeh, D. F., Chen, X., Latzko, P., Malz, M., Gaida, M. M., Felix, K., Ladu, S., Singer, S., Pinna, F., Gretz, N. et al. (2013). Yes-associated protein up-regulates jagged-1 and activates the NOTCH pathway in human hepatocellular carcinoma. *Gastroenterology* **144**, 1530-1542.e12. doi:10.1053/j.gastro.2013.02.009

Tu, F., Sedzinski, J., Ma, Y., Marcotte, E. M. and Wallingford, J. B. (2018). Protein localization screening in vivo reveals novel regulators of multiciliated cell development and function. *J. Cell Sci.* **131**, jcs206565. doi:10.1242/jcs.206565

Varelas, X. (2014). The Hippo pathway effectors TAZ and YAP in development, homeostasis and disease. *Development* **141**, 1614-1626. doi:10.1242/dev.102376

Volckaert, T., Yuan, T., Chao, C.-M., Bell, H., Sitaula, A., Szimmtenings, L., El Agha, E., Chanda, D., Majka, S., Bellusci, S. et al. (2017). Fgf10-Hippo epithelial-mesenchymal crosstalk maintains and recruits lung basal stem cells. *Dev. Cell* **43**, 48-59.e5. doi:10.1016/j.devcel.2017.09.003

Wickam, H. (2016). *ggplot2: Elegant Graphics for Data Analysis*. New York: Springer-Verlag.

Yang, Y., Riccio, P., Schotsaert, M., Mori, M., Lu, J., Lee, D.-K., García-Sastre, A., Xu, J. and Cardoso, W. V. (2018). Spatial-temporal lineage restrictions of embryonic p63+ progenitors establish distinct stem cell pools in adult airways. *Dev. Cell* **44**, 752-761.e4. doi:10.1016/j.devcel.2018.03.001

Yimlamai, D., Christodoulou, C., Galli, G. G., Yanger, K., Pepe-Mooney, B., Gurung, B., Shrestha, K., Cahan, P., Stanger, B. Z. and Camargo, F. D. (2014). Hippo pathway activity influences liver cell fate. *Cell* **157**, 1324-1338. doi:10.1016/j.cell.2014.03.060

You, Y., Richer, E. J., Huang, T. and Brody, S. L. (2002). Growth and differentiation of mouse tracheal epithelial cells: selection of a proliferative population. *Am. J. Physiol. Lung Cell. Mol. Physiol.* **283**, L1315-L1321. doi:10.1152/ajplung.00169.2002

Yu, F. X. and Guan, K. L. (2013). The hippo pathway: regulators and regulations. *Genes Dev.* **27**, 355-371. doi:10.1101/gad.210773.112

Zhang, K., Qi, H.-X., Hu, Z.-M., Chang, Y.-N., Shi, Z.-M., Han, X.-H., Han, Y.-W., Zhang, R.-X., Zhang, Z., Chen, T. et al. (2015). YAP and TAZ take center stage in cancer. *Biochemistry* **54**, 6555-6566. doi:10.1021/acs.biochem.5b01014

Zhao, B., Tumaneng, K. and Guan, K.-L. (2011). The Hippo pathway in organ size control, tissue regeneration and stem cell self-renewal. *Nat. Cell Biol.* **13**, 877-883. doi:10.1038/ncb2303

Zhao, B., Li, L., Wang, L., Wang, C.-Y., Yu, J. and Guan, K. L. (2012). Cell detachment activates the Hippo pathway via cytoskeleton reorganization to induce anoikis. *Genes Dev.* **26**, 54-68. doi:10.1101/gad.173435.111

Zhao, R., Fallon, T. R., Saladi, S. V., Pardo-Saganta, A., Villoria, J., Mou, H., Vinarsky, V., Gonzalez-Celeiro, M., Nunna, N., Hariri, L. P. et al. (2014). Yap tunes airway epithelial size and architecture by regulating the identity, maintenance, and self-renewal of stem cells. *Dev. Cell* **30**, 151-165. doi:10.1016/j.devcel.2014.06.004

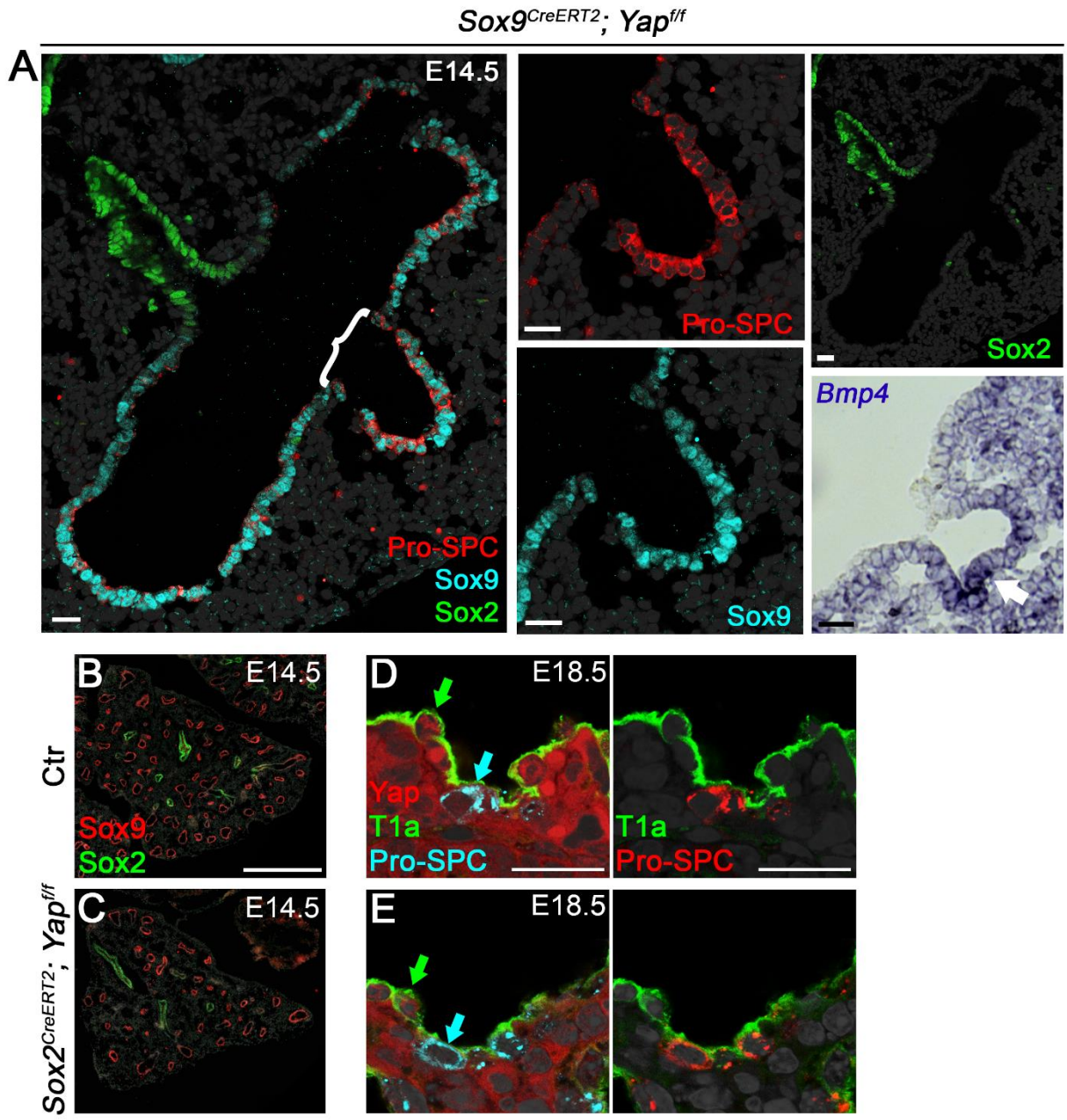

Figure S1. Effects of Yap disruption in Sox9 progenitors during lung development.

(A) immunofluorescence of Pro-SPC, Sox9 and Sox2 and in situ hybridization of *Bmp4* (bottom right panel) in E14.5 *Sox9*^{CreERT2}*; Yap*$^{f/f}$ lung: preserved early distal cell fate in the epithelium of aberrant distal cysts (bracket, arrow). **(B-E)** Representative IF images

from control and mutant lungs showing similar proximal-distal distribution of Sox2-Sox9 signals at E14.5 and similar expression of distal differentiation markers (T1a and Pro-SPC: alveolar type 1 and 2, respectively; arrows) at E18.5. DAPI: in grey. Scale bars: (B-C): 100µm, (A, D-E): 20µm.

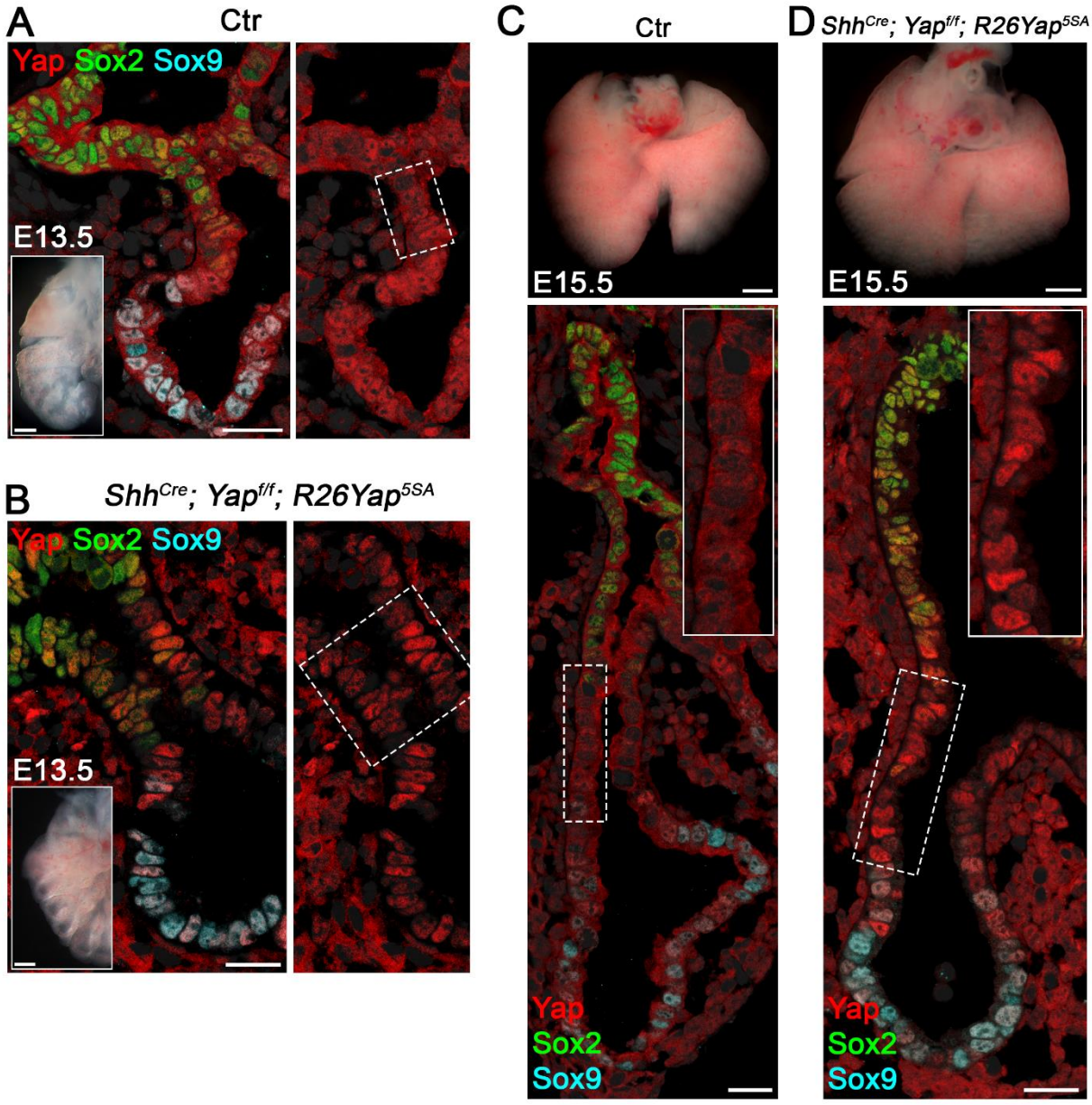

Figure S2. Constitutive nuclear Yap expression allows normal proximal-distal patterning during lung development.

(A-D) Immunofluorescence of Yap, Sox2 and Sox9 and wholemount images (insets in A, B and upper panels of C, D) of E13.5 and E15.5 control and *Shh^{Cre}; Yap$^{f/f}$; R26Yap^{5SA}* lungs. Proper branching and proximal-distal epithelial cell fate in Yap-

deficient mutants expressing constitutively active nuclear Yap. Boxed regions depict the transition zone between Sox9 and Sox2 compartments, highlighting the nuclear Yap localization in *R26Yap*^{5SA}+ mutants (B, D) as compared to WT samples (A, C). DAPI: grey in all panels. Scale bars in (A-D, IF stains): 20µm, (A-B, insets): 200µm, (C-D, wholemounts): 500µm.

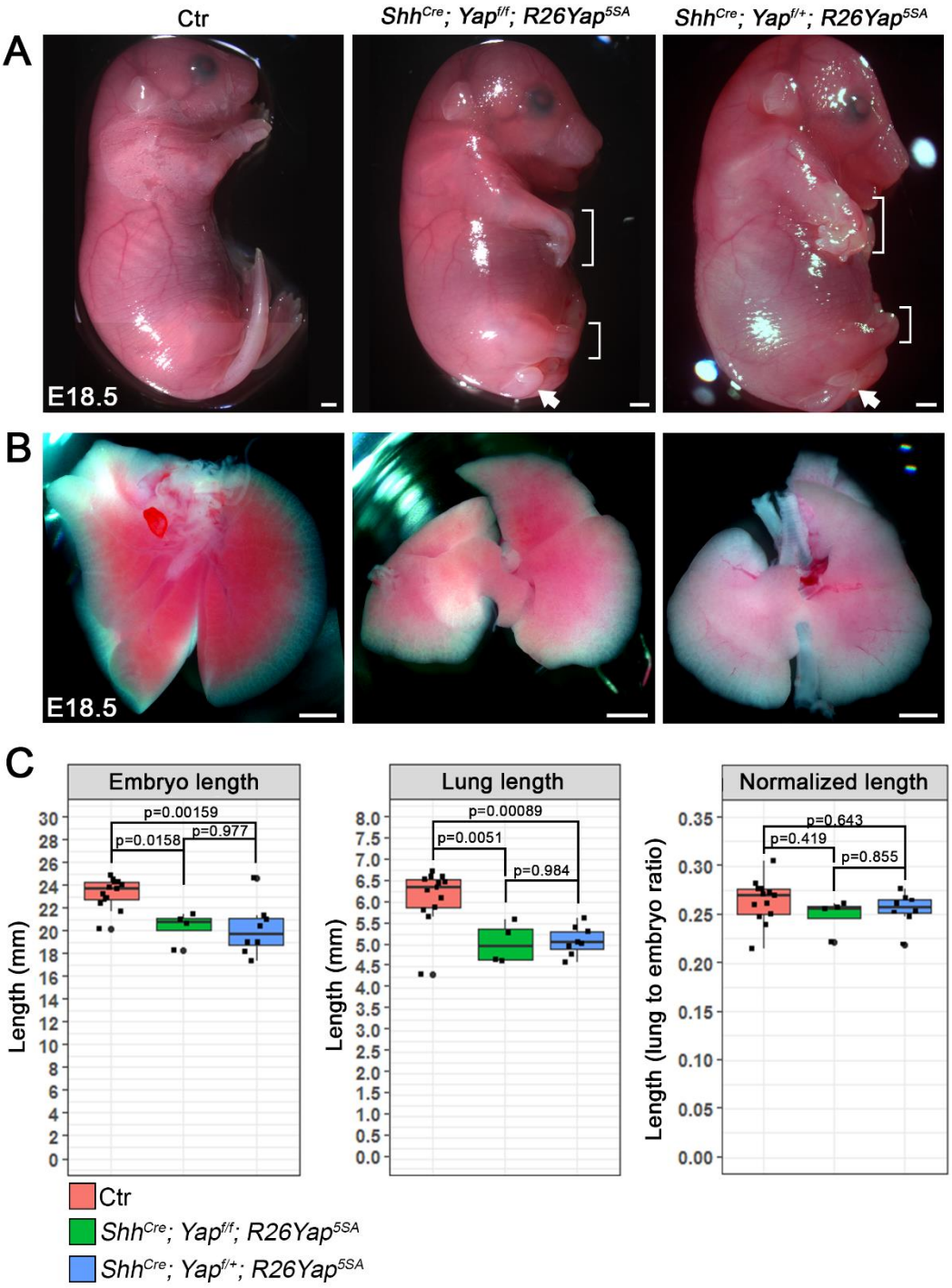

Figure S3. Constitutively active nuclear Yap rescues lung morphogenesis but causes severe developmental defects elsewhere in Yap-deficient mutants.

(A-B) Representative wholemount images of E18.5 control, *Shh^{Cre}; Yap$^{f/f}$; R26Yap^{5SA}*

and *Shh*^{Cre}*; Yap*$^{f/+}$*; R26Yap*^{5SA} mutants. *R26Yap*^{5SA} causes limb (brackets) and tail (arrow) defects, but rescues the aberrant lung morphogenetic phenotype. **(C)** Measurements of E18.5 embryo length, lung length and lung length normalized by embryo length: control (n=13) lungs are bigger than *Shh*^{Cre}*; Yap*$^{f/f}$*; R26Yap*^{5SA} (n=4) and *Shh*^{Cre}*; Yap*$^{f/+}$*; R26Yap*^{5SA} (n=8) lungs, but lung to body ratio does not differ. Graphs: boxplots depict median, 1st and 3rd quartiles (box, middle, lower and upper lines), minimum and maximum values (whiskers) and outliers (dots). p-values calculated by one-way ANOVA followed by post-hoc Tukey test. Scale bars: 1mm.

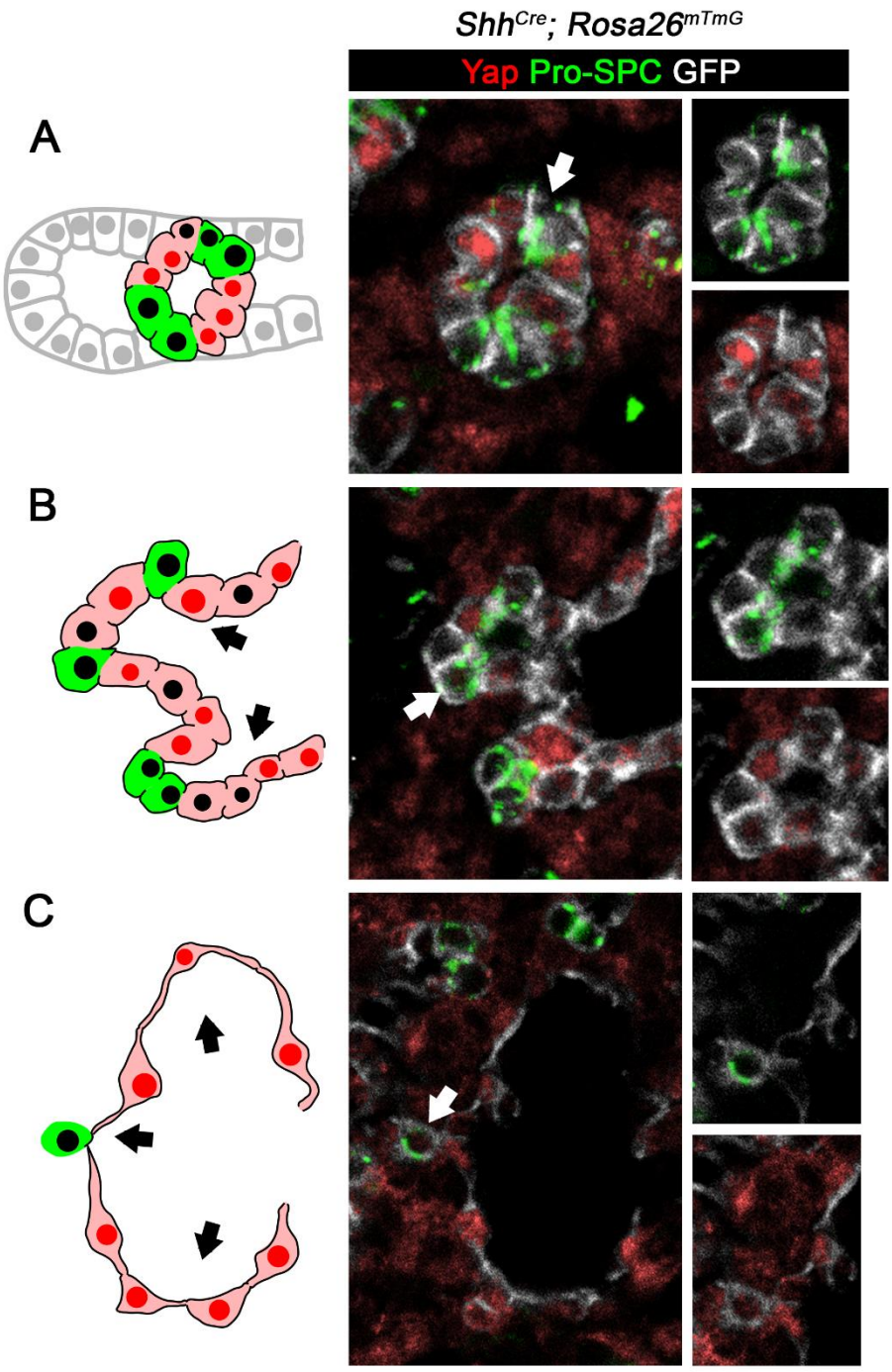

Figure S4. Distal progenitors expressing nuclear Yap flatten and are excluded from the program of alveolar type 2 (AT2) differentiation.

(A-C) Left panels: schematics of the morphogenetic and differentiation events in distal

buds undergoing sacculation. Right panels: Immunofluorescence (IF) staining for Yap, Pro-SPC (arrows) and GFP in *Shh*^{Cre}*; Rosa26*^{mTmG} lungs (GFP in grey marking cell membranes). Note Pro-SPC+ distal epithelial cells protrude from lumen (arrows), do not flatten and are nuclear Yap-negative.

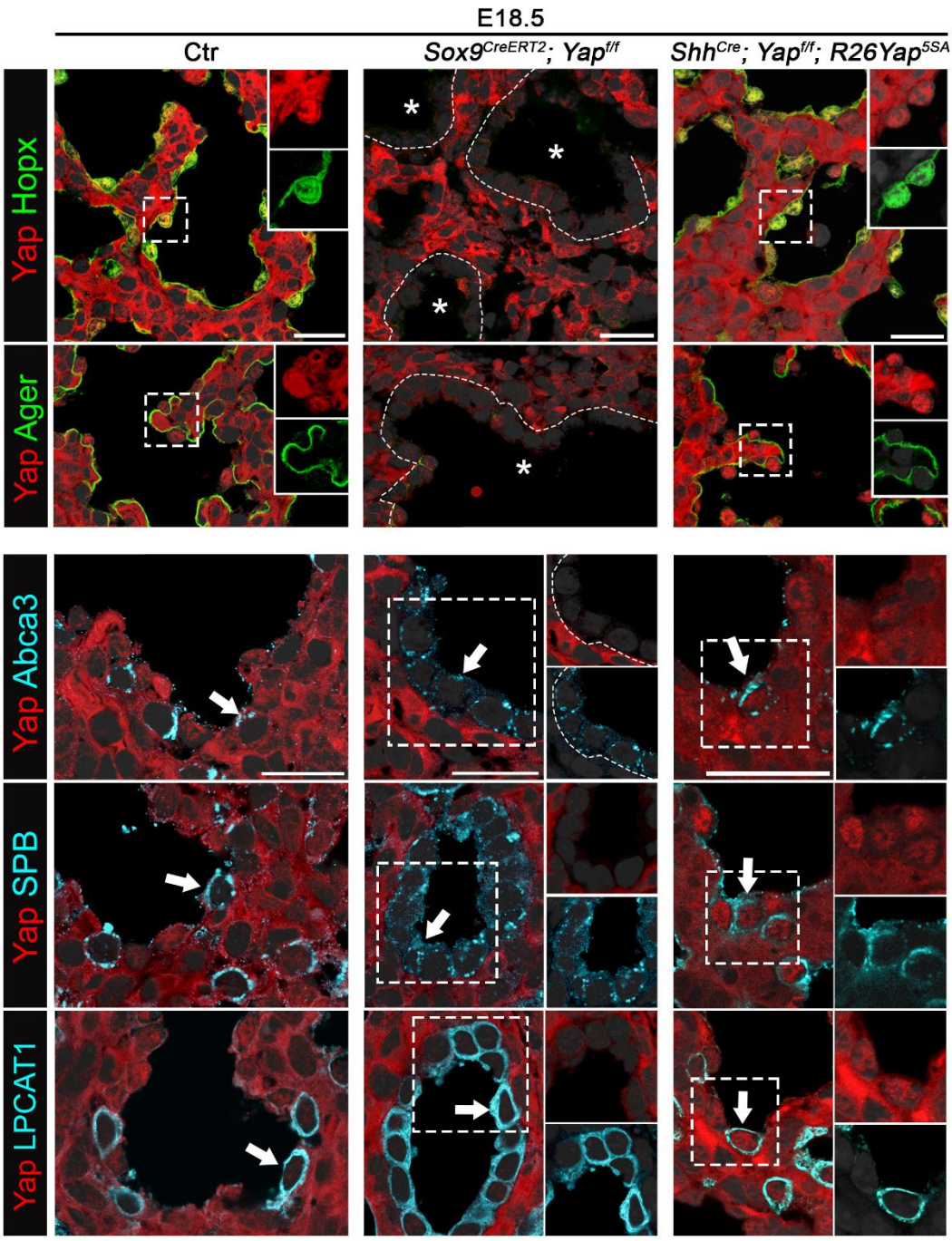

Figure S5. Constitutively active Yap rescues the AT1 differentiation program in Yap-deficient lungs.

(A-B) Immunofluorescence of Yap with AT1 (Hopx, Ager), or AT2 (Abca3, SPB or LPCAT1) markers in E18.5 control, *Sox9^{CreERT2}; Yap$^{f/f}$* and *Shh^{Cre}; Yap$^{f/f}$; R26Yap^{5SA}*

lungs. Insets: single channel images from boxed areas. Loss of Yap in Sox9+ progenitors prevents AT1 differentiation (asterisks in A). Neither disruption of Yap nor constitutive expression of nuclear Yap prevents AT2 cell formation (arrows in B). DAPI: grey in all panels. Scale bars: 20μm

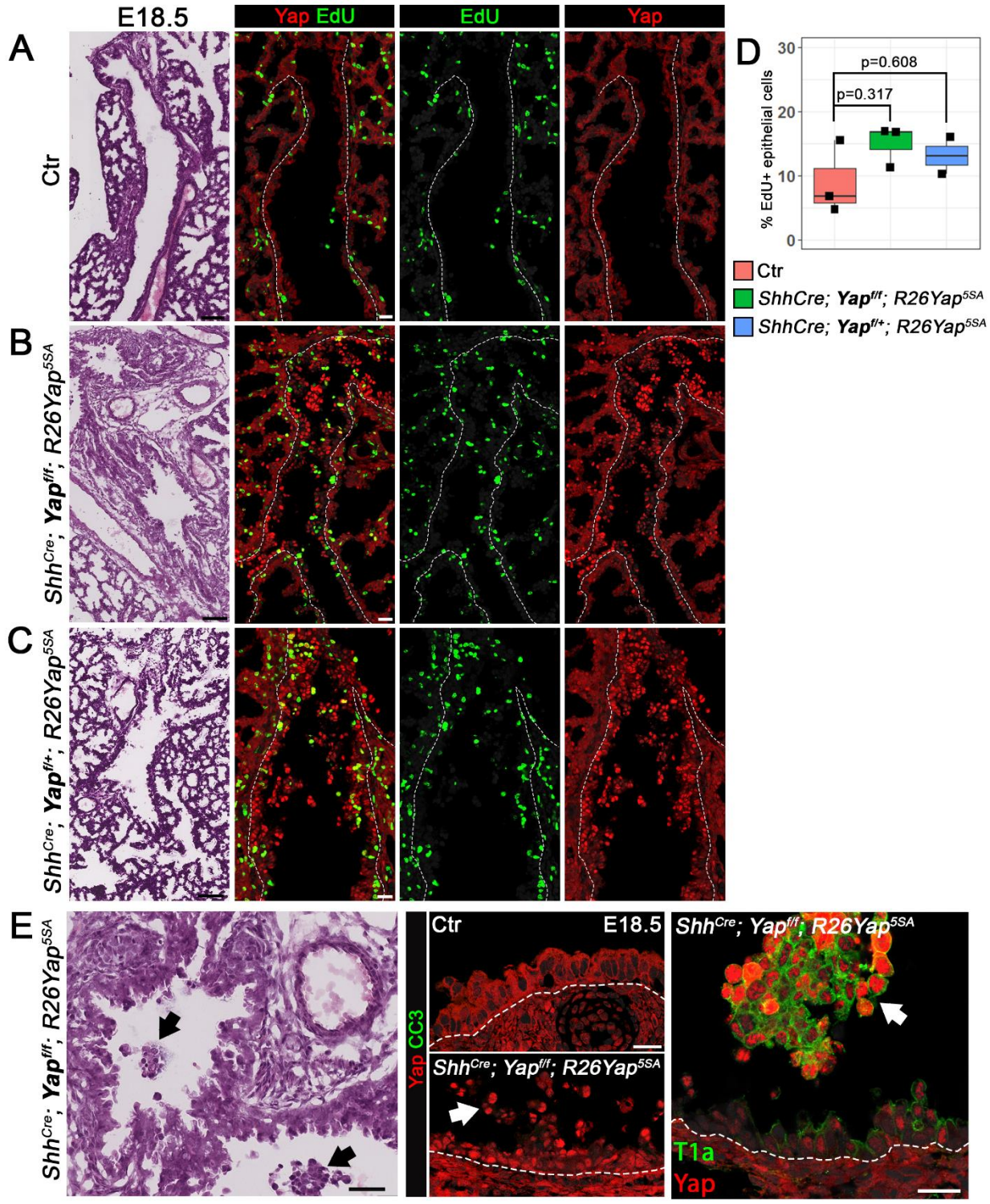

Figure S6. Nucleocytoplasmic shuttling of Yap is required to maintain the integrity of the developing airway epithelium.

(A-C) H&E and Yap, EdU immunofluorescence (IF) in E18.5 control (n=3) (A), *Shh^{Cre};*

Yap$^{f/f}$*; R26Yap*^{5SA} (n=3) (B) and *Shh*^{Cre}*; Yap*$^{f/+}$*; R26Yap*^{5SA} lungs (n=2) (C). **(D)** Quantitative analysis: percent of Edu incorporation (epithelium only); boxplots: median, 1st and 3rd quartile (box), minimum and maximum (whiskers) values. Loss of epithelial integrity and presence of luminal cell clumps without significant increase in proliferation in airways expressing Yap unable to localize to the cytoplasm. n=3 lungs for control and *Shh*^{Cre}*; Yap*$^{f/f}$*; R26Yap*^{5SA}, n=2 lungs for *Shh*^{Cre}*; Yap*$^{f/+}$*; R26Yap*^{5SA} lungs. p-values calculated through one-way ANOVA followed by post-hoc Tukey test. **(E)** Representative H&E and IF staining of large airway in *Shh*^{Cre}*; Yap*$^{f/f}$*; R26Yap*^{5SA} lungs showing luminal cell clumps strongly labeled with Yap and T1a without evidence of apoptosis (negative for cleaved caspase 3, CC3). DAPI: grey in all panels. Dashed lines denote basement membrane. Scale bars: 100μm H&E; 20μm IF (A-C IF, E all panels).

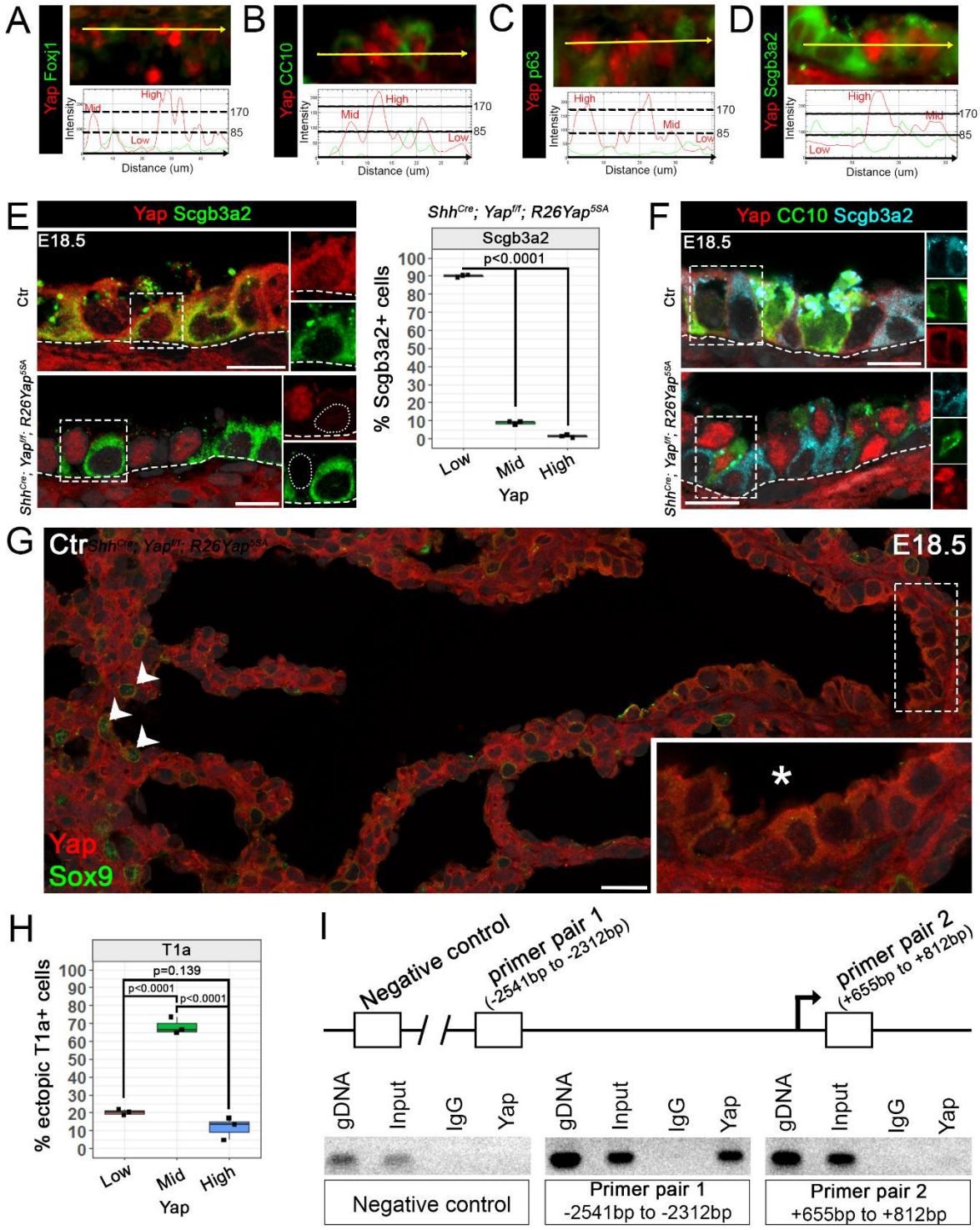

Figure S7. Nuclear Yap co-localization with airway differentiation markers, Yap^{5SA} differentially affects expression of secretory markers during airway epithelial differentiation and regulation of *Sox2* expression in airway epithelial progenitors. (A-D) Strategy for quantification of fluorescent signal intensity in lung sections of E18.5 *Shh^{Cre}; Yap$^{f/f}$; R26Yap^{5SA}* lungs double-labelled with Yap and Foxj1 (A), CC10 (B), p63 (C) or scgb3a2 (D). Graphs: values of signal intensity (arbitrary units) over a distance (µm, yellow line) defining three categories of Yap signal levels (low, intermediate, high; see methods) and their association with the differentiation markers indicated. **(E)** Immunofluorescence for Yap and Sgb3a2 in E18.5 control and *Shh^{Cre}; Yap$^{f/f}$; R26Yap^{5SA}* lungs demonstrating Scgb3a2+ cells do not colocalize with Yap^{high} and quantitation represented as boxplot. n=3 lungs per genotype. p-values obtained by one-way ANOVA followed by post-hoc Tukey test. Dotted lines in IF single channel panels denote nuclei. **(F)** Immunofluorescence stain for Yap, Scgb3a2 and CC10 in E18.5 control and *Shh^{Cre}; Yap$^{f/f}$; R26Yap^{5SA}* lungs: CC10 and Scgb3a2 label different cell populations that respond differently to Yap^{high} expression. **(G)** IF staining of Yap and Sox9 in E18.5 WT lung. Airway epithelial cells are Sox9 negative (inset, asterisk). DAPI: grey in all panels. **(H)** Boxplot demonstrating that ectopic T1a+ cells in the airway don't co-localize with low nuclear Yap levels. n=3 lungs per genotype. p-values obtained by one-way ANOVA followed by post-hoc Tukey test. **(I)** ChIP-PCR analysis for Sox2 in adult airway progenitors (tracheal basal cells) showing Yap binding to the *Sox2* gene locus selectively in the *Sox2 promoter* containing Yap-TEAD binding site (primer pair 1) but not elsewhere (within Sox2 coding region (primer pair 2) or unrelated region ~100kb upstream of *Sox2* locus; see methods). When expanded in culture these progenitors express nuclear Yap endogenously; Sox2 is a marker of airway progenitor cell fate (Mahoney et al., 2014; Que et al., 2009). Boxplots depict median, 1st and 3rd quartile (box, middle, lower and upper lines) and minimum and maximum (whiskers)). DAPI: grey in E-G. Scale bars in E-F represent 10µm; (G) 20µm.